Article

Developmental Cell

A single-cell census of mouse limb development identifies complex spatiotemporal dynamics of skeleton formation

Graphical abstract

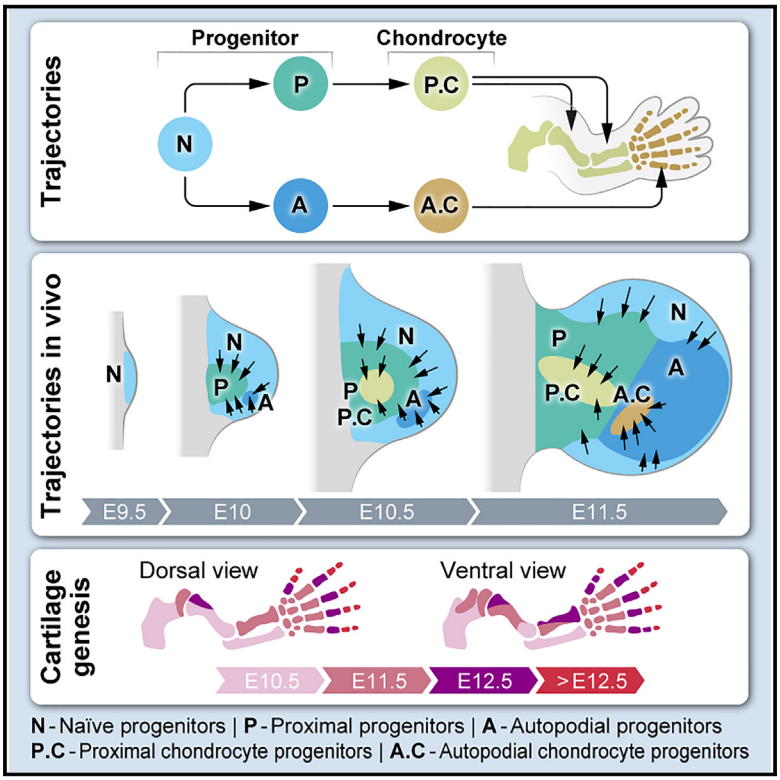

Highlights

- *Msx1* is a marker for naive, multipotent limb mesenchymal progenitors
- Naive progenitors transition into proximal and autopodial progenitors
- This transition occurs simultaneously at different locations for several days
- Chondrocyte differentiation is also a progressive and non-sequential process

Authors

Svetlana Markman, Mor Zada, Eyal David, Amir Giladi, Ido Amit, Elazar Zelzer

Correspondence

ido.amit@weizmann.ac.il (I.A.), eli.zelzer@weizmann.ac.il (E.Z.)

In brief

Markman, Zada, et al. propose a model for vertebrate limb development that is opposed to the prevailing model of proximodistal patterning. They show that the skeleton forms progressively and simultaneously at multiple foci along the developing limb, and this involves the transition of *Msx1*$^{+}$ naive progenitors into either proximal or autopodial progenitors.

Markman et al., 2023, Developmental Cell *58*, 1–17
April 10, 2023
https://doi.org/10.1016/j.devcel.2023.02.013

CellPress

Please cite this article in press as: Markman et al., A single-cell census of mouse limb development identifies complex spatiotemporal dynamics of skeleton formation, Developmental Cell (2023), https://doi.org/10.1016/j.devcel.2023.02.013

Developmental Cell

CellPress

Article

A single-cell census of mouse limb development identifies complex spatiotemporal dynamics of skeleton formation

Svetlana Markman,[1,3] Mor Zada,[2,3] Eyal David,[2] Amir Giladi,[2] Ido Amit,[2,4,*] and Elazar Zelzer[1,4,5,*]
[1]Department of Molecular Genetics, Weizmann Institute of Science, Rehovot 7610001, Israel
[2]Department of Immunology, Weizmann Institute of Science, Rehovot 7610001, Israel
[3]These authors contributed equally
[4]These authors contributed equally
[5]Lead contact
*Correspondence: ido.amit@weizmann.ac.il (I.A.), eli.zelzer@weizmann.ac.il (E.Z.)
https://doi.org/10.1016/j.devcel.2023.02.013

SUMMARY

Limb development has long served as a model system for coordinated spatial patterning of progenitor cells. Here, we identify a population of naive limb progenitors and show that they differentiate progressively to form the skeleton in a complex, non-consecutive, three-dimensional pattern.

Single-cell RNA sequencing of the developing mouse forelimb identified three progenitor states: naive, proximal, and autopodial, as well as *Msx1* as a marker for the naive progenitors. *In vivo* lineage tracing confirmed this role and localized the naive progenitors to the outer margin of the limb, along the anterior-posterior axis. Sequential pulse-chase experiments showed that the progressive transition of *Msx1*$^+$ naive progenitors into proximal and autopodial progenitors coincides with their differentiation to *Sox9*$^+$ chondroprogenitors, which occurs along all the forming skeletal segments. Indeed, tracking the spatiotemporal sequence of differentiation showed that the skeleton forms progressively in a complex pattern. These findings suggest an alternative model for limb skeleton development.

INTRODUCTION

Limb development has long served as a model system for studying organ formation. Extensive research has identified key components in the genetic program that controls both patterning and differentiation of the different limb tissues, as well as the complex signaling involved in regulating this genetic program.[1–7] These studies have produced the basic concepts of how progenitor cells pattern and differentiate along the three axes to form a complex functional organ.[8–10]

The mouse forelimb starts to develop around E9.5 as a small outgrowth from the body wall. Initially, the limb bud comprises seemingly homogeneous mesenchymal cells covered by a layer of ectoderm. At the distal end, along the anterior-posterior (AP) border, the ectoderm thickens to form the apical ectodermal ridge (AER). As development proceeds, the limb is elongated and the hand plate is formed. Concurrently, the development of the limb skeleton is initiated, as mesenchymal cells form condensations that prefigure the future skeletal elements.

The vertebrate limb skeleton is organized in three segments: stylopod, containing humerus in the forelimb or femur in the hindlimb; zeugopod, comprising radius and ulna or tibia and fibula; and autopod, comprising the wrist or ankle and digits. Surgical removal of the AER during early wing-bud development resulted in severe truncation of the distal elements. Moreover, the later the AER was removed, the more distal elements were formed. These findings led to the perception that the skeletal elements of the limb form in a proximal-to-distal order under the regulation of the AER.[11,12] Several models have attempted to explain this mode of development.[8] The progress zone model is named after a distal domain under the AER, where limb progenitor cells are postulated to be located.[11,12] According to this model, the longer these progenitors spend in the progress zone, the more distal their progeny become. Once the cells exit this domain, their fate is determined. Thus, the first cells to leave the progress zone form the stylopod, the next to leave form the zeugopod, and the cells that exit last form the autopod.[11–13] An alternative model posits that progenitors of the limb segments are specified early in development, organized in three parallel stripes, and then expand progressively in a proximodistal order.[14,15] The two-signal model suggests that proximal and autopod progenitors are specified by two opposing signals deriving from the flank and AER, respectively. Later on, as the limb bud grows, a third domain of the zeugopod is formed in the middle.[16–18]

Recently, several works have studied mouse and chick limb development at single-cell resolution.[19–23] Despite their findings, fundamental aspects of this process are still missing. For example, the identity of limb progenitors and their spatial distribution are unclear, as we lack marker genes to identify them. The temporal changes the transcriptome of these progenitors undergo

Please cite this article in press as: Markman et al., A single-cell census of mouse limb development identifies complex spatiotemporal dynamics of skeleton formation, Developmental Cell (2023), https://doi.org/10.1016/j.devcel.2023.02.013

during development and the sequence by which they differentiate to form the limb skeleton have yet to be uncovered too.

In this work, we establish a single-cell census of the developing limb and characterize limb progenitors. We identified three populations of limb progenitors, namely naive, proximal, and autopodial. We established *Msx1* as a marker for the naive progenitors and their location in the outer margin of the developing limb, along the AP axis. We then showed that these *Msx1*$^+$ naive progenitors transit progressively and simultaneously into either proximal or autopodial progenitors. Moreover, the progressive contribution of these progenitors to the forming skeleton occurs simultaneously all along the proximal-distal (PD) axis of the limb. Finally, temporal analysis of the differentiation of *Msx1* lineage cells identified that the skeleton forms in a complex non-consecutive three-dimensional (3D) pattern, which extends to the level of the single element.

RESULTS

Single-cell RNA sequencing provides a comprehensive cellular and molecular census of the major mesenchyme-derived cell types of the developing limb

To identity limb mesenchymal progenitor cells and their differentiation paths, we generated transcriptional maps of mesenchymal lineages in the developing limb between E10.5 and E14.5 by applying massively parallel single-cell RNA-seq (MARS-seq). To ensure representation of the different cell types and differentiation states, including rare subpopulations, we combined lineage and reporter-based single-cell analysis using *Sox9* and *Scx*, the earliest known markers for skeletal and tendon cells, respectively.[24–26]

At E10.5, we sampled a *Sox9-GFP* transgenic mouse line and collected both *Sox9*$^+$ and negative cells. Because *Sox9* marks multiple cell types,[27–30] to follow the dynamics of different lineages and to ensure the representation of tendons, we generated a compound mouse model containing *Sox9-CreER*^{T2},[28] *tdTomato*,[31] and *Scx-GFP*.[32] Tamoxifen was administered at different developmental stages between E9.5 and E12.5, and samples were harvested 48 h later. Thus, we sampled four cell populations: tdTomato-positive (*Sox9*$^+$ skeletal lineage), GFP-positive (*Scx*$^+$ tendon cells), tdTomato-GFP double-positive cells, and double-negative cells (other progenitors). Then, 32,000 quality-filtered cells (see STAR Methods) were subjected to MARS-seq. We used the MetaCell algorithm[33] to identify homogeneous and robust groups of cells, referred to as metacells (MCs; see STAR Methods). MCs of non-lateral plate mesoderm origin, such as red blood cells, muscle cells, and ectoderm-derived cells, were excluded from the analysis (STAR Methods). The remaining 250 MCs were grouped into 12 molecularly distinct populations (Figures 1B–1F and S1).

To annotate the clusters, we performed differential gene expression analysis using the chondrocyte markers *Sox9*, *Col2a*, *Wwp2*, and *Col9a2* and fibroblast markers *Col1a1*, *Col3a1*, *Scx*, *Osr1*, *Dcn*, and *Lum*.[24–26,34–39] Results showed that subsets C1–C6 represent chondrocyte subpopulations (Figures 1F, S1J, and S2; Data S1), and groups CT0–CT2 represent connective tissue fibroblast subpopulations (Figures 1F, S1J, and S3; Data S1). Cells in subsets P1 and P3 expressed neither fibroblast nor chondrocyte markers and were therefore annotated as mesenchymal progenitors (Figures 1C–1F). A large gene signature defined these progenitor types, including *Hist1h2ao* (Data S2), which was expressed by P1–P3 cells but not by any of the differentiated cell types (Figures 1E and 1F). P1 cluster was characterized by co-expression of *Msx1* and *Lhx9*, transcription factors (TFs) that are expressed in limb mesenchyme and play a key role in limb patterning;[40–42] *Hmga2*, which is widely expressed in undifferentiated cells during embryogenesis;[43,44] *Asb4*; and *Igdcc3*, which was suggested to play a role in early embryogenesis.[45] Interestingly, these progenitors lacked a spatial signature.

P2 cells expressed a gene module that largely overlapped with that of P1; however, they lacked the expression of *Msx1* and *Lxh9*. Instead, they expressed high levels of *Shox2*, a TF that acts as a patterning gene at the proximal limb bud;[46] *Dlk1*; *Zfhx3-4*; *Scx*; and *Col3a1*. The P3 subset was characterized by high expression of *Hoxd13*, *Msx1*, *Lhx9*, and *Aldh1a2*. The known role of these genes in regulating autopod patterning suggests that this cluster represents progenitors of the autopod.[47,48]

Subsets CT0–CT2 were characterized by the expression of *Col5a1*, *Col3a1*, *Col1a1*, and *Osr1*, all of which are markers of connective tissue/tendon.[39,49] In addition, these cells also expressed *Lgals1*, which was implicated in modulating cell-cell and cell-matrix interactions. Other identified markers were *Kctd12*, encoding for a potassium channel, and tropomyosin (*Tpm1*) (Figures 1F and S1). Interestingly, CT0 cells did not express the key tendon marker *Scx*. Instead, this cluster shared several genes with P3, including markers such as *Msx1*, *Hoxd13*, and *Aldh1a2* (Figures 1F, S1J, and S3), suggesting that P3 autopod progenitors give rise to CT0 cells. CT1 and CT2 were both characterized by the expression of tendon markers *Scx*, *Dcn*, and *Lum*.[26,39] In addition, cells of both clusters expressed the TF *Zfhx4*. *Zfhx3* marked CT1 cells,[50] whereas CT2 was marked by high expression of *Dlk1*, *Igfbp5*, and *Sparc*.[49,51]

In the chondrocyte compartment (Figures 1F, S1, and S2; Data S1), subsets C1 and C2 displayed low expression levels of cartilage-specific ECM genes (cECM), such as *Col2a1*, *Col9a1-3*, *Col11a1-2*, and *Hapln1*, indicating the early differentiation stage of these clusters.[24,25,52,53] In line with this, C1 displayed high expression levels of *Asb4*, *Shox2*, *Hmga2*, and *Igdcc3*, which marked cluster P2, suggesting that cluster C1 originates from P2 cells. Cluster C2 displayed high expression of the TFs *Ebf1* and *Sfrp2*, a soluble modulator of Wnt signaling, and of the autopod marker *Hoxd13*, suggesting that this cluster represents early autopodial chondrocytes. Subset C3 displayed expression of *Hoxd13*, intermediate levels of cECM genes, and high *Tgfbi* expression,[54] suggesting that it represents more mature autopodial chondrocytes. Subset C4 displayed intermediate expression levels of cECM genes in combination with several fibroblast markers; specifically high expression of *Col1a1*; and low expression of *Scx*, *Col3a1*, and *Lgals1*. These results suggest a chondro-tendinous identity of these cells.[29,49,55] Subset C5 displayed high expression levels of cECM genes along with the autopod marker *Hoxd13*, thus representing the most mature state of autopodial chondrocytes. Subset C6 displayed the highest expression levels of all cECM genes, consistent with the most differentiated chondrocytes.

To elucidate the temporal dynamics of identified cell populations, we examined cell-type composition during development

Please cite this article in press as: Markman et al., A single-cell census of mouse limb development identifies complex spatiotemporal dynamics of skeleton formation, Developmental Cell (2023), https://doi.org/10.1016/j.devcel.2023.02.013

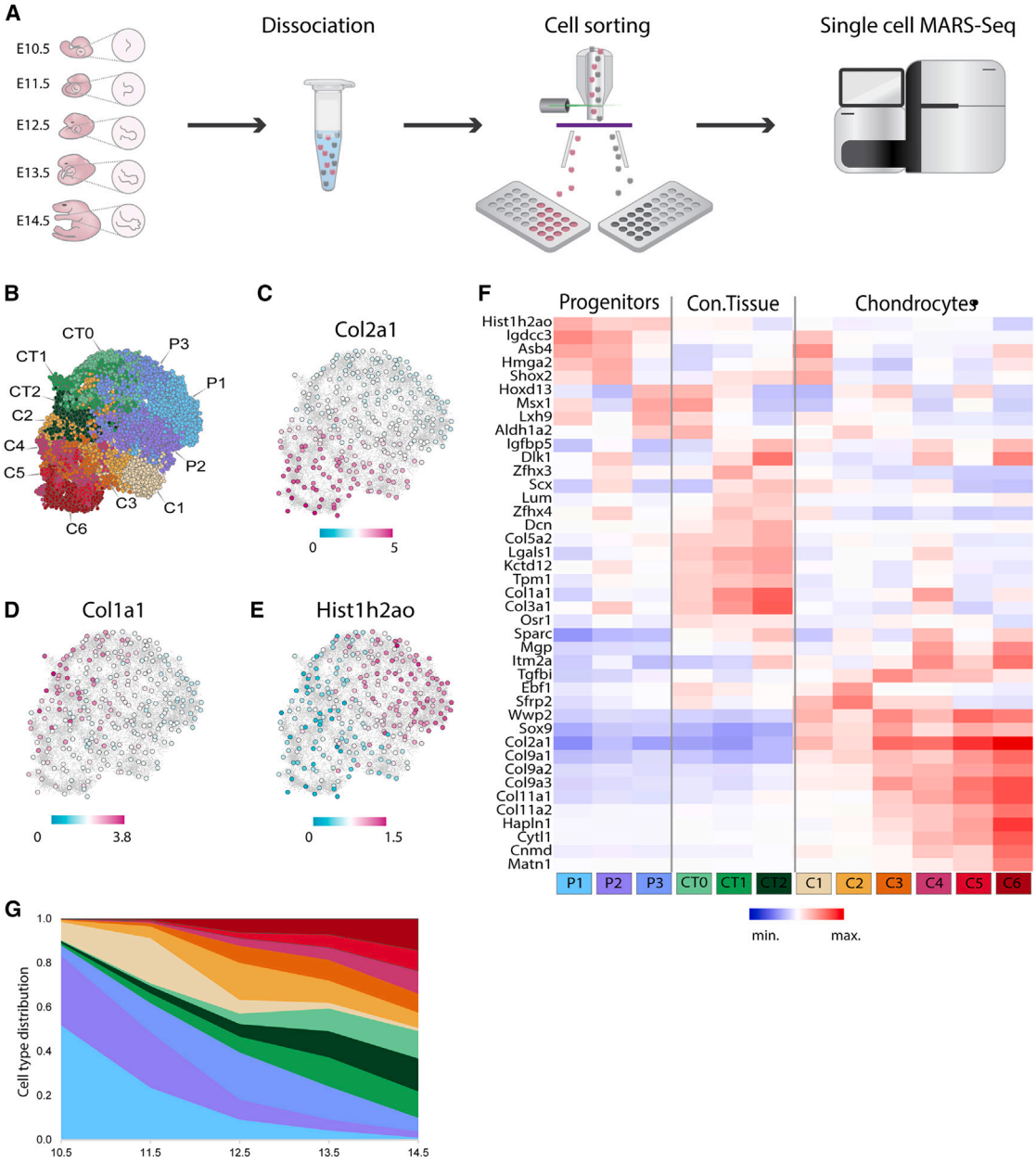

Figure 1. Single-cell RNA sequencing of mouse forelimb mesenchymal cells during embryonic development

(A) Scheme showing the experimental design. At E10.5, *Sox9-GFP* embryos from 3 females were used to separate between GFP-positive and -negative cells. Additionally, cells were collected from *Sox9-CreER^{T2};tdTomato;Scx-GFP* embryos from 2 females without Cre activation. E11.5–E14.5 forelimbs were from *Sox9-CreER^{T2};tdTomato;ScxGFP* embryos (E11.5–E12.5, 4 females per stage; E13.5–E14.5, 5 females per stage). *Sox9*$^{+}$ cells were labeled by tamoxifen administration 48 h before harvesting. Collected cells were sorted into tdTomato^{+}GFP^{-}, tdTomato^{-}GFP^{+}, double-positive and double-negative cells. Forelimbs of embryos from the same litter were pooled together. Overall, we analyzed six forelimbs per litter at E10.5 (total 30 forelimbs) and E11.5 (total 24 forelimbs), four forelimbs per litter at E12.5 (total 16 forelimbs) and E13.5 (total 20 forelimbs), and two forelimbs from one E14.5 embryo per litter (total 10 forelimbs).

(B) *k*-nearest neighbors (*k*-NN) graph of 26,131 mesenchymal cells.

(C–E) The 250 metacells were subdivided into three main cell populations, as shown by $\log_2$-fold change in gene expression of *Col2a1* (C), *Col1a1* (D), and *Hist1h2ao* (E) genes projected onto the *k*-NN graph.

(F) Heatmap showing $\log_2$-fold change in expression of differentially expressed marker genes in 12 transcriptionally distinct cell populations.

(G) Plot showing the percentage of the different cell types at each developmental stage, color-coded as in (B) and (F).

See also Figures S1–S3, Table S1, and Data S1 and S2.

Please cite this article in press as: Markman et al., A single-cell census of mouse limb development identifies complex spatiotemporal dynamics of skeleton formation, Developmental Cell (2023), https://doi.org/10.1016/j.devcel.2023.02.013

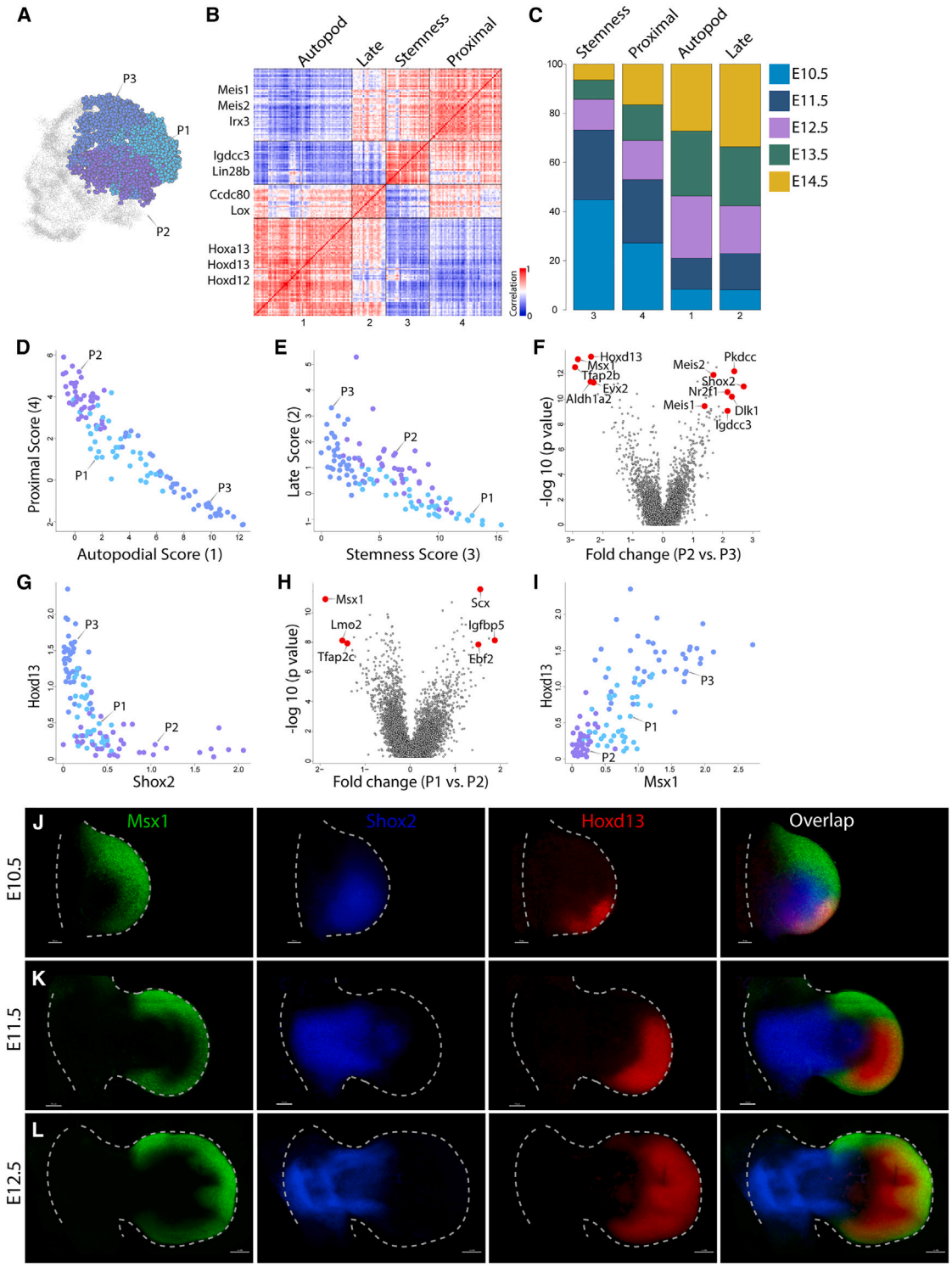

Figure 2. Characterization of mesenchymal progenitor cells

(A) *k*-NN graph of 10,241 progenitor cells, grouped into three subsets. Dots represent single cells, which were annotated and color-coded as in Figure 1B.

(B) Heatmap showing hierarchical clustering of 175 genes that were most variably expressed by progenitor cells into four modules, based on gene-gene Pearson's correlation. Representative genes are indicated for each gene module.

(C) Graph showing the relative contributions of cells at various developmental stages to the total gene expression in each module.

(D) Scatterplot showing the distribution of autopodial (x axis) and proximal (y axis) scores in progenitor metacells.

(E) Scatterplot showing the distribution of stemness (x axis) and late (y axis) scores in progenitor metacells.

(legend continued on next page)

Please cite this article in press as: Markman et al., A single-cell census of mouse limb development identifies complex spatiotemporal dynamics of skeleton formation, Developmental Cell (2023), https://doi.org/10.1016/j.devcel.2023.02.013

and found dramatic changes (Figure 1G; Table S1). While P1 was the most abundant cell population at E10.5, it virtually disappeared by E13.5. Proximal progenitors (P2) constantly decreased from E10.5 until E14.5. Conversely, autopodial progenitors (P3) have dramatically increased by E12.5 and then started to decline. Early proximal chondrocytes (C1) were already identified at E10.5, became more abundant at E11.5, and declined thereafter. Early autopodial chondrocytes (C2) first appeared at E11.5, concurrently with the appearance of tendon fibroblasts CT1 and CT2, and became more abundant at E12.5 when more mature chondrocytes (C3–C6) and CT0 cells appeared. At E13.5, we observed a decrease in C2, whereas the abundance of mature chondrocytes (C3–C6), CT1, CT2, and CT0 continued to increase. By E14.5, C2 continued to decrease, and C3 and CT1 displayed a slight reduction, while C4–C6, CT2, and CT0 further increased.

Overall, these data identify the main mesenchyme-derived cells types in the developing limb, as well as specific markers for these types. We identified three populations of progenitors, including autopodial and proximal progenitors and a third progenitor population that lacks spatial signature. Interestingly, we failed to identify a zeugopodial progenitor population. Finally, the gradual reduction in progenitor cells and increase in differentiated cells suggest a progressive differentiation process in the developing limb.

Characterization of limb progenitors

To gain insight into transcriptional and molecular mechanisms regulating the three identified progenitor subpopulations (Figure 2A), we computationally extracted annotated MCs from these cells and computed the Pearson's correlation coefficients for each pair of genes across all cells (see STAR Methods). Hierarchical clustering of the correlation matrix (Figure 2B; Data S3) identified four gene modules. Module 1 was enriched for components of signaling pathways such as TGF-β/activin and BMP (*Bmp2*, *Gdf5*, *Dlx5*, *Dlx6*, *Inhba*, and *Bambi*), Wnt (*Wnt5a*), and Fgf (*Fgf12* and *Sp9*), as well as for retinoic acid synthesis enzymes (*Aldh1a2* and *Rdh10*). This module also contained several TFs that regulate limb patterning (*Msx1*, *Msx2*, *Lhx2*, and *Lxh9*) as well as TFs that are essential specifically for autopod patterning, such as *Hoxa13*, *Hoxd13*, *Hoxd12*, *Tfap2a*, and *Tfap2b*,[56,57] thus representing an autopodial genetic program. Module 2 was enriched with genes involved in matrix formation (*ccdc80*, *Lox*, and *Eln*) and calcium binding proteins (*Egfl6*, *Sned1*, *Sparc*, and *Piezo2*) as well as with Wnt signaling components *Dkk2* and *Fzd8*, likely representing a progressive stage of cell differentiation.

Module 3 was enriched for several signaling pathways, such as Wnt (*Rspo4*) and BMP (*Grem1*), and a subset of homeobox genes including *Hoxd4*, *Hoxd8*, *Hoxd9*, *Hoxa11*, and *Shox2*. Interestingly, this module was also enriched with genes associated with the maintenance of pluripotency and stem cell function, including *Igdcc3*, *Sall4*, *Lin28b*, *Tfapc2*, and *Trim71*, consistent with a stemness genetic program.[57–67] Module 4 was enriched for signaling pathways such as Igf (*Igf2*, *Igfbp5*, *Igfbp3*, and *Igf1*) and Wnt (*Ror1* and *Dact1*). Additionally, it contained proximally expressed genes such as *Meis1*, *Meis2*, *Pkdcc*, *Meox1*, *Pitx2*, *Emx2*, and *Irx3*, thus representing a proximal gene program.[17,68–75] Interestingly, module 4 also contained genes associated with tendon and connective tissue formation, such as *Scx*, *Tcf15*, *Osr2*, and *Cxcl12*.[76,77]

We next examined the temporal activity of these four modules (Figure 2C). Results showed that 8% of the autopodial module 1 gene expression came from E10.5 cells, 12% from E11.5 cells, and 25%–27% from E12.5–E14.5 cells. These results suggest that autopodial gene program is detectable already at E10.5 cells and becomes more prominent at E12.5–E14.5. In module 2, 8% of the gene expression was associated with E10.5 cells, with a constantly increasing contribution at later developmental stages (15% at E11.5, 19% at E12.5, 24% at E13.5, and 34% at E14.5), suggestive of a late genetic program. In the stemness module 3, 45% of gene expression was associated with E10.5 cells, followed by a decline in contribution at later stages (28% at E11.5, 12% at E12.5, 8% at E13.5, and 6% at E14.5). These results indicate that cells turn off the expression of stemness genes as development proceeds. Proximal genes of module 4 were expressed throughout this period, as shown by the contribution of cells at all developmental stages (27% E10.5, 26% E11.5, 16% E12.5, 14% E13.5, and 16% E14.5).

Next, we utilized our gene module information to classify the three identified progenitor populations by calculating scores of each module for each MC. Examination of proximal (4) vs. autopodial (1) module scores showed that MCs of proximal P2 and autopodial P3 were completely separated (Figure 2D). P2 was enriched with proximal module genes, whereas P3 was enriched with autopodial module genes, further confirming our annotation. Interestingly, P1 MCs had low levels of both proximal and autopodial scores, with some MCs overlapping with proximal or autopodial MCs. This suggests that these cells transit into proximal and autopodial progenitor states. Moreover, P1 MCs had higher stemness module (3) scores, as compared with P2 and P3, which had intermediate and high late module (1) scores, respectively (Figure 2E), further supporting the naive state of P1. Finally, examination of proximal and stemness scores showed a clear separation between the three progenitor groups. P1 was characterized by high-to-intermediate stemness score combined with low proximal scores, whereas P2 was characterized by intermediate stemness scores combined with high proximal

(F) Volcano plot showing differentially expressed genes between P2 and P3 cells, presented as expression fold change (x axis) and p value (y axis, $-\log_{10}$ scale). The five most significantly differentially expressed genes and the two established proximal markers *Meis1* and *Meis2* are indicated by red dots.
(G) Scatterplot showing the differences in *Shox2* (x axis) and *Hoxd13* (y axis) expression across progenitor metacells.
(H) Volcano plot showing differentially expressed genes between P1 and P2 cells, presented as expression fold change (x axis) and p value (y axis, $-\log_{10}$ scale). The three most significantly differentially expressed genes are indicated by red dots.
(I) Scatterplot showing the differences in *Msx1* (x axis) and *Hoxd13* (y axis) expression across progenitor metacells.
(J–L) Maximum intensity projection (MIP) images of E10.5 (J), E11.5 (K), and E12.5 (L) whole-mount forelimbs stained for *Msx1* (green), *Shox2* (blue), and *Hoxd13* (red) mRNA, using *in situ* HCR and imaged by light sheet microscopy. At each stage, n = 2.
See also Figure S4, Data S1 and S3, and Videos S1, S2, and S3.

Please cite this article in press as: Markman et al., A single-cell census of mouse limb development identifies complex spatiotemporal dynamics of skeleton formation, Developmental Cell (2023), https://doi.org/10.1016/j.devcel.2023.02.013

scores. P3 displayed the lowest levels of both proximal and stemness scores (Figures S4A and S4B).

To identify the *in vivo* spatiotemporal distribution of these progenitors during limb development, we searched for specific markers for the three progenitor populations. For that, we first analyzed the most differentially expressed genes between proximal and autopodial progenitors. As shown in Figures 2F and 2G and Data S1, *Shox2* and the known proximal markers *Meis1* and *Meis2* were upregulated in proximal progenitors, whereas *Tfap2b*, *Hoxd13*, *Hoxa13*, and *Msx1* were among the most differentially expressed genes in autopodial progenitors. We selected *Shox2* and *Hoxd13* for our *in situ* experiments because of their higher expression levels. Naive progenitors displayed significantly lower levels of *Hoxd13* (1.3-fold, p = 10.7 $-\log_{10}$; Data S1). A comparison of gene expression between naive and proximal subpopulations showed that *Msx1* was among the most differentially expressed genes by P1 cells (Figure 2H; Data S1). Because *Msx1* was also expressed by P3 cells, we examined the combination of *Msx1* and *Hoxd13*. As seen in Figure 2I, this combination clearly separated between P1 and P3 MCs. Thus, we defined *Msx1*$^+$/*Hoxd13*$^-$ cells as naive progenitors, *Shox2*$^+$ cells as proximal progenitors, and *Msx1*$^+$/*Hoxd13*$^+$ as autopodial progenitors.

Next, we conducted whole-limb triple *in situ* hybridization chain reaction (HCR) using *Msx1*, *Shox2*, and *Hoxd13* probes. As seen in Figure 2J, at E10.5, *Msx1* was expressed in the outer margin of the limb forming an arc-like pattern along the AP axis. The arc extended both dorsally and ventrally from the AP midline, more so dorsally (Figures S4C–S4E). At the anterior-proximal side of the arc, the *Msx1* expression domain was the widest (Figures 2J, S4F, and S4G). At the dorsal side, the most posterior *Msx1* expression domain overlapped with the *Hoxd13* expression domain, demarcating the location of the autopodial progenitors (Figures 2J, S4H, and S4I; Video S1). *Shox2* proximal progenitors were found at the core of the limb bud, encircled by the *Msx1* expression domain.

At E11.5 (Figures 2K and S4J–S4P), the arc-like pattern of *Msx1* expression along the AP axis was maintained, as were the size asymmetries along the AP and dorsal-ventral (DV) axes. The overlap between *Msx1* and *Hoxd13* expression domains expanded dorsally and ventrally as well as anteriorly, occupying the most distal front of the limb (Video S2). The *Shox2* expression domain extended throughout most of the proximal limb segment.

At E12.5 (Figure 2L), the *Msx1* arc-like expression domain was still visible. *Msx1* and *Hoxd13* expression domains (Video S3) occupied the interdigital space and most of the outer margin of the autopod, with the exception of the anterior region of the developing thumb and a small posterior region, which were positive only for *Msx1* (Figures S4Q and S4R). The *Shox2* expression domain occupied most of the proximal limb segment. Areas of overlap between *Shox2* and *Msx1* and between *Msx1* and *Hoxd13* were observed for several days, supporting the transition of P1 cells into either P2 or P3 cells, as suggested by our analysis.

Together, these results suggest that P1 represents naive multipotent progenitor cells, which are marked by *Msx1* and are located in the outer margin of the forming limb. These progenitors differentiate into P2 proximal progenitors, marked by *Shox2*, and P3 autopodial progenitors, which are co-marked by *Msx1* and *Hoxd13*. The observed coexistence of P2 and P3 cells at E10.5–E12.5 suggests that this transition occurs over several developmental days. Because P2 and P3 represent two spatially distinct domains, our data also suggest that the transition of P1 cells into P2 and P3 cells occurs in two locations in parallel. In the following, the temporally continuous transition will be referred to as "progressive," whereas the spatially parallel transition will be termed "simultaneous."

Msx1 marks the naive progenitors of the limb

A central hypothesis raised by our single-cell data is that the TF *Msx1* marks the most naive limb mesenchymal progenitors. If so, this TF should be expressed at the onset of limb development, and its lineage should give rise to all mesenchyme-derived tissues, including cartilage, tendon, and muscle connective tissue. To test this prediction, we first studied the expression of *Msx1* at E9.5, the onset of limb development. As seen in Figure 3A and in agreement with previous studies,[78] *Msx1* expression was observed in the cells of the forming forelimb. To examine directly the contribution of the *Msx1* lineage to the different mesenchymal limb tissues, we utilized the *Msx1-CreER*^{T2} knockin mouse line[79] crossed with *Rosa26-tdTomato*[31] and *Scx-GFP*[32] mice. As seen in Figures 3B–3F, a single dose of tamoxifen at E9.5 marked cells of the entire skeleton, tendons, and muscle connective tissue in the E14.5 forelimb. These results support the hypothesis that *Msx1* marks the naive progenitors and confirm the high efficiency of the *Msx1-CreER*^{T2} knockin allele in activating the *Rosa26-tdTomato* reporter.

To demonstrate *in vivo* the progressive transition of *Msx1*$^+$ naive progenitors into proximal and autopodial progenitors, we combined sequential pulse-chase genetic lineage tracing, using the *Msx1-CreER*^{T2}*;Rosa26-tdTomato* mice, with whole-mount *in situ* HCR for *Msx1* and *Shox2*. The sequential short (30 h) chase periods identified the temporal dynamics of *Msx1*$^+$ cell differentiation, whereas *in situ* HCR for *Msx1* provided the position of the naive progenitors at the end of the chase. To mark proximal progenitors, we performed HCR for *Shox2*.

At E10.5, while restricted *Msx1* expression was observed at the outer margin of the limb along the AP axis, tdTomato signal was detected throughout the limb, including in *Msx1*$^+$ cells. *Shox2* expression was observed in *tdTomato*$^+$*Msx1*$^-$ cells, which were surrounded by *tdTomato*$^+$*Msx1*$^+$ cells (Figure 4A). These results indicate that at that stage, some of the pulsed cells maintained their naive state mostly at the margin of the limb, whereas the center was occupied by *Msx1* lineage cells that had lost their naive state and adopted a new fate, some as proximal progenitors. At E11–E11.5, *Msx1* expression in the outer margin of the limb was maintained, whereas tdTomato-expressing cells were found in the anterior-proximal domain but not in the proximal posterior domain. *Shox2* expression was observed in the center of the limb, overlapping the tdTomato signal except at the posterior side. These results demonstrate the transition of *Msx1* naive progenitors into proximal progenitors between E10.5 and E11.5 (Figures 4B and 4C). At E12.5, *Msx1* expression was observed in the autopod margin and interdigital space, demarcating metacarpals 2–5. tdTomato-expressing cells were found in the autopod margin and a few in the anterior-proximal domain. *Shox2* expression was observed in the proximal limb, stylopod,

Please cite this article in press as: Markman et al., A single-cell census of mouse limb development identifies complex spatiotemporal dynamics of skeleton formation, Developmental Cell (2023), https://doi.org/10.1016/j.devcel.2023.02.013

CellPress

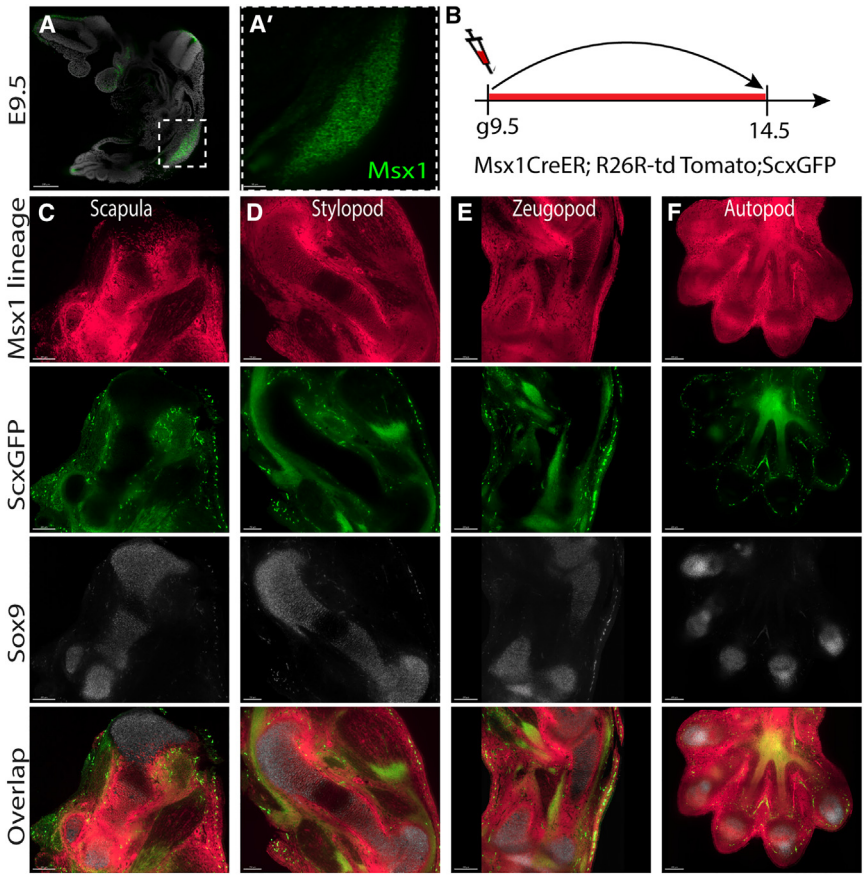

Figure 3. *Msx1* marks the naive progenitors of the limb

(A) Optical section through E9.5 embryo stained for *Msx1* mRNA (green), using *in situ* HCR, counterstained with DAPI (gray) and imaged by light sheet microscopy (n = 2). Dashed white square demarcates the forelimb. (A′) Magnification of dashed white square in (A).

(B) Scheme showing the design of the pulse-chase cell lineage experiment (g, gavage).

(C–F) Optical sections through scapula (C), stylopod (D), zeugopod (E), and autopod (F) (n = 3). Tendons are visualized by *Scx-GFP* (green), cartilage is visualized by *in situ* HCR staining of *Sox9* mRNA (gray). Whole forelimbs were imaged by light sheet microscopy.

and zeugopod, where the anterior and posterior sides adjacent to the autopod overlapped partially with the tdTomato signal (Figure 4D), demonstrating that the transition was still taking place between E11.5 and E12.5. Expression of *Msx1* also by autopodial P3 progenitors raised the possibility that proximal P2 cells are derived from P3 as well. However, P3 cells also expressed *Hoxa13*, whose lineage was previously shown to contribute only to the autopod,[47] negating this possibility.

Finally, we examined cell fate stability of *Msx1*$^+$naive progenitors during development. For that, we compared gene expression between progenitors from different time points. As seen in Figures S5A–S5F, *Igdcc3*, *Asb4*, and *Hmga2* were found to be highly expressed by E10.5 and E11.5 P1 cells, as compared with later stages, whereas E12.5 P1 cells displayed higher expression of the autopodial marker *Hoxd13*. A comparison between E12.5 and E13.5 P1 cells did not identify differentially expressed genes. Overall, this analysis indicates that naive progenitors largely maintain their transcriptional program, with mild change.

Together, these results confirm that *Msx1*$^+$ progenitors give rise to all mesenchyme-derived tissues of the limb. We demonstrated the progressive transition of *Msx1*$^+$ naive progenitors to proximal progenitors, which takes place for several days, concomitantly with autopod development. Moreover, we showed that the addition of new proximal progenitors took place mainly on the anterior side and to a lesser extent on the posterior side.

Differentiation of *Msx1* lineage cells to *Sox9*$^+$ chondroprogenitors occurs progressively and simultaneously along the different skeletal segments

Having found progressive differentiation of *Msx1*$^+$ naive progenitors, we proceeded to study the differentiation dynamics of this lineage into chondroprogenitors by comparing the expression of *Msx1* to that of *Sox9*, the earliest known chondro-osteogenic marker.[24,27,35] For that, we established a chondrogenic gene module anchored to *Col2a1*, a *bona fide* chondrogenic marker,[80] and used it to compute a chondrogenic score. Cells from each day were ordered by chondrogenic score and binned into 65 bins. The mean expression of *Sox9* and *Msx1* was calculated for each bin, and trend line and confidence interval were calculated (see STAR Methods). This analysis identified that at all sampling time points, cells with low chondrogenic score expressed high levels of *Msx1* and low levels of *Sox9*. As cells progressed through differentiation, *Sox9* expression was upregulated as expected, while *Msx1* expression was downregulated (Figures 5A and 5B). The differentiation sequence of *Msx1*$^+$ naive progenitors into fully differentiated chondrocytes was further supported by pseudotime and lineage reconstruction analysis using Slingshot (Figures S6A–S6F).

To validate this, we performed *in situ* HCR for *Sox9* and *Msx1* on E10.5–E12.5 forelimbs. As seen in Figures S6G–S6I and in agreement with the single-cell results, the expression domains of *Msx1* and *Sox9* were mutually exclusive, with slight overlap at the borders likely representing the transitional stage.

Our data analysis indicated that the differentiation of *Msx1* naive progenitors into *Sox9*-expressing chondroprogenitors has taken place on each of the examined days, suggesting that it is a progressive process. To demonstrate *in vivo* the spatiotemporal dynamics of this process, we combined sequential short (30 h) pulse-chase experiments, using the *Msx1-CreER*^{T2}*;Rosa26-tdTomato* mice, with whole-mount *in situ* HCR for *Msx1* and *Sox9*. At E10.5, *Msx1* lineage cells populated the entire limb. *Sox9* expression was observed in the center of

Please cite this article in press as: Markman et al., A single-cell census of mouse limb development identifies complex spatiotemporal dynamics of skeleton formation, Developmental Cell (2023), https://doi.org/10.1016/j.devcel.2023.02.013

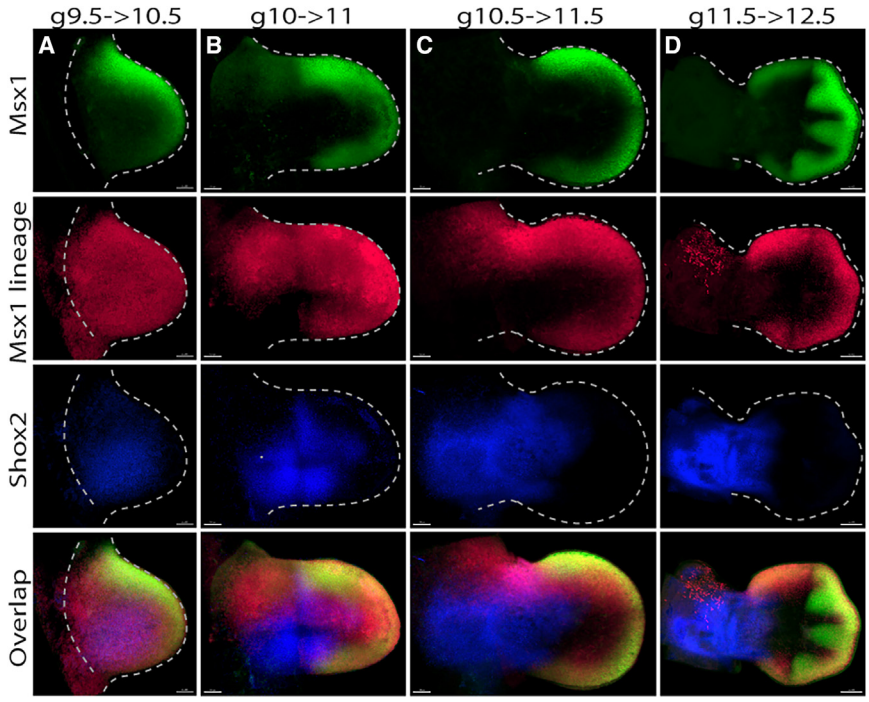

Figure 4. *Msx1*$^+$ naive limb progenitors progressively differentiate into proximal or autopodial progenitors

Pulse-chase experiment using *Msx1-CreER*^{T2}*; Rosa26-tdTomato* mice. *Msx1*$^+$ cells were labeled by tamoxifen administration at E9.5 (A), E10.5 (B), E11 (C), or E11.5 (D); and forelimbs were harvested 30 h later. MIP images of whole-mount forelimbs stained for *Msx1* (green) and *Shox2* (blue) mRNA, using *in situ* HCR, and imaged by light sheet microscopy. At each stage, n = 2; g, gavage.
See also Figure S5.

the limb, within a *tdTomato*$^+$*Msx1*$^-$ domain, which was surrounded by *tdTomato*$^+$*Msx1*$^+$ cells at the margin (Figure 5C). Examination at E11.5 showed that *Msx1* lineage cells populated most of the limb, excluding the most proximal posterior domain. The *Sox9* expression domain was observed in the center of the limb. Interestingly, the *Sox9* expression domain overlapped with *tdTomato*$^+$*Msx1*$^-$ cells along the entire forming skeleton, mostly on the anterior side (Figures 5D and 5D′). *tdTomato*$^+$*Msx1*$^+$ cells were located at the autopod margin, surrounding the distal *Sox9* expression domain. At E12.5, *Msx1* lineage cells were observed at the autopod margin, with a small proximal extension on the anterior side. *Sox9* expression demarcated the humerus, radius, ulna, and five metacarpals. *Sox9* expression overlapped with *tdTomato*$^+$*Msx1*$^-$ cells at the distal anterior radius, metacarpals 1 and 5, and tips of metacarpals 2–4. Areas of overlap between *Sox9* expression and *tdTomato*$^+$*Msx1*$^+$ cells were detected in the lateral side of metacarpals 2–4 and at all metacarpal tips (Figures 5E and 5E′).

Overall, these results support the temporally progressive differentiation of *Msx1* lineage cells not only into proximal and autopodial progenitors but also into *Sox9*$^+$ chondroprogenitors. Moreover, this process is not restricted spatially, but it rather occurs simultaneously along all segments of the developing skeleton.

The skeleton forms progressively and non-consecutively in a complex three-dimensional pattern

Our observation of simultaneous differentiation of *Msx1*$^+$ naive progenitors into chondroprogenitors in all the developing skeletal segments prompted us to reexamine the order by which these segments form. The finding that *Msx1* expression is lost once the naive progenitors differentiate provided us with a unique opportunity to address this question. We postulated that the first element to form would be composed of descendants of progenitors that lost *Msx1* expression first, whereas the last element to form would derive from progenitors that were last to lose *Msx1* expression. To follow temporally the loss of *Msx1* expression by naive progenitors, we performed consecutive pulse-chase lineage tracing experiments by administering single doses of tamoxifen to *Msx1-CreER*^{T2}*; Rosa26-tdTomato*mice at E9.5, E10.5, E11.5, or E12.5. To determine the spatial distribution of tdTomato-positive cells in the forming skeleton, we cleared limbs of E13.5 embryos and imaged them using light sheet microscopy.

As seen in Figure 6A, tamoxifen administration at E9.5 resulted in tdTomato labeling of the entire skeleton. However, pulsing at E10.5 (Figure 6B) resulted in loss of tdTomato signal in most of the scapula, ventral humerus (Figure S7A), and radius. tdTomato signal was observed in the acromion, humeral head and deltoid tuberosity, dorsal humerus, ulna, and in the entire autopod (Figures 6B and S7B). Pulsing at E11.5 (Figure 6C) resulted in loss of tdTomato signal in acromion and humeral shaft and in metacarpals of digits 3 and 4 (Figure S7C). Still, tdTomato signal was detected at the humeral head and deltoid tuberosity, radius, and most of the digits. Finally, following pulsing at E12.5 (Figure 6D), tdTomato signal was lost in the radius and metacarpals, but it remained at the tips of the growing digits (Figure S7D). These results indicated that the skeleton forms progressively in a complex pattern and not linearly along the PD axis.

Next, we examined in greater detail the tdTomato signal in the humerus and radius. As seen in Figures 6E and 6M‴, in the humerus, pulsing at E10.5 led to the loss of tdTomato signal at the ventral side from head to medial epicondyle, whereas the dorsal side was tdTomato-positive from head to lateral epicondyle. Following pulsing at E11.5, the areas of the humerus that lost tdTomato signal were in the dorsal shaft and lateral epicondyle, whereas the deltoid tuberosity and the dorsal side of humeral head were still tdTomato-positive (Figures 6J–6N‴). In the radius, tamoxifen administration at E10.5 resulted in tdTomato labeling throughout the bone (Figures 6O–6S‴). However, pulsing at E11.5 resulted in loss of tdTomato signal in almost the entire ventral side, with few labeled cells on its distal tip (Figure 6T). On the dorsal side, the proximal posterior side of the

Please cite this article in press as: Markman et al., A single-cell census of mouse limb development identifies complex spatiotemporal dynamics of skeleton formation, Developmental Cell (2023), https://doi.org/10.1016/j.devcel.2023.02.013

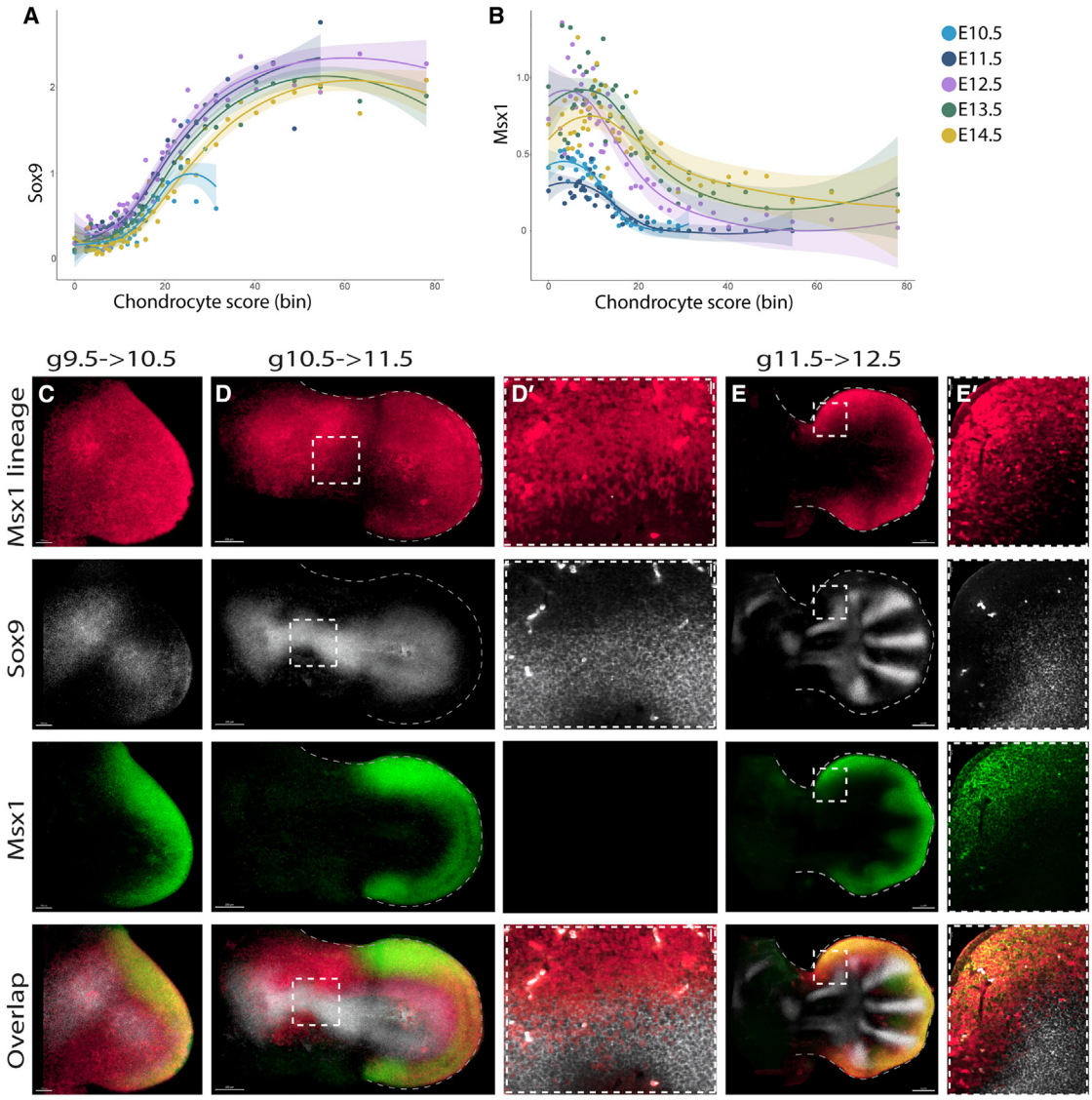

Figure 5. Spatiotemporal analysis of the differentiation of *Msx1*$^+$ progenitors into *Sox9*$^+$ cells

(A and B) Graphs showing the expression of *Sox9* (A) and *Msx1* (B) by progenitor cells and chondrocytes that were ordered by chondrogenic scores.

(C–E) Pulse-chase experiment using *Msx1-CreER*^{T2}*;Rosa26-tdTomato* mice. *Msx1*$^+$ cells were labeled by tamoxifen administration at E9.5 (C), E10.5 (D) and (D′), or E11.5 (E) and (E′); and forelimbs were harvested 30 h later. MIP images of whole-mount forelimbs stained for *Msx1* (green) and *Sox9* (gray) mRNA, using *in situ* HCR, and imaged by light sheet microscopy. (D') and (E') are magnifications of the dashed white squares in (D) and (E), respectively. At each stage, n = 2; g, gavage.

See also Figure S6.

radius was mostly tdTomato-negative, while the anterior side still displayed extensive labeling (Figures 6U–6X‴). These results indicate that the ventral side of the radius forms first, followed by a diagonal AP direction of dorsal radius formation. Thus, the results from these two bones are consistent with a complex pattern of skeletal formation (Figures 6Y and 6Z).

To validate the results of the *Msx1* lineage experiments, we examined the spatiotemporal dynamics of chondroprogenitor differentiation in the limb by following the induction of *Sox9* expression. For that, we used the *Sox9-CreER*^{T2} mice, which were previously shown to efficiently drive the expression of *Rosa26-lacZ* reporter in the developing skeleton.[28] Because both our single-cell and lineage studies have shown that at E10.5, only part of the *Sox9* chondroprogenitors were differentiated (Figure 6B), we activated Cre activity at this time point and harvested the limbs 30 and 72 h afterward. E11.5 whole limbs were stained for *Sox9* mRNA using *in situ* HCR, whereas E13.5 whole limbs were stained for SOX9 protein and imaged using light sheet microscopy. At 30 h post-induction (Figures 7A–7E‴), tdTomato signal was observed in most of the scapula, and only on the ventral-posterior side of the humerus and ulna, whereas the radius and autopod were tdTomato-negative. At 72 h (Figures 7F–7J″), tdTomato labeling was seen in most of the scapula, the entire humeral shaft, and ulna; however, the acromion, humeral head, deltoid tuberosity, lateral

Please cite this article in press as: Markman et al., A single-cell census of mouse limb development identifies complex spatiotemporal dynamics of skeleton formation, Developmental Cell (2023), https://doi.org/10.1016/j.devcel.2023.02.013

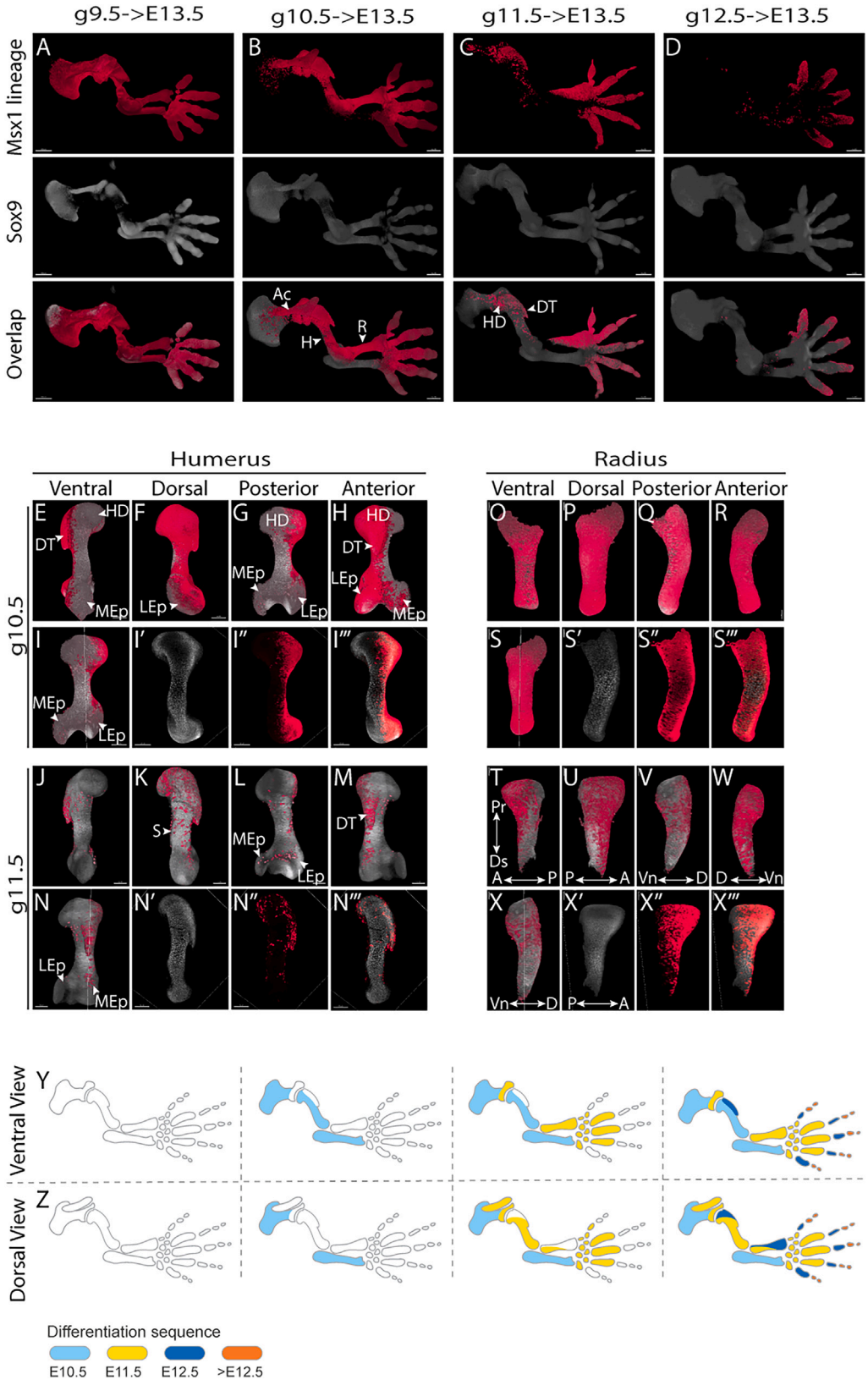

(legend on next page)

Please cite this article in press as: Markman et al., A single-cell census of mouse limb development identifies complex spatiotemporal dynamics of skeleton formation, Developmental Cell (2023), https://doi.org/10.1016/j.devcel.2023.02.013

and medial epicondyles, elbow, and most of the radius and digits were tdTomato-negative. These results further support the notion that the skeleton forms non-consecutively in a complex pattern that involves not only the PD axis but also the DV and AP axes, extending to the level of the single element.

DISCUSSION

In this work, we revisit the long-standing question of the spatiotemporal sequence of limb development using modern molecular tools. We generated a comprehensive cellular census of the limb mesenchymal cell lineages during development. Using this census, we identified a population of naive progenitors and their progressive and simultaneous transition into proximal and autopodial progenitors. We establish *Msx1* as a marker of naive progenitors and localize them to the outer margin of the developing limb, along the AP axis. We then showed that the descendants of these progenitors progressively contribute to the entire forming skeleton. Finally, temporal analysis of the differentiation of naive progenitors identified that the skeleton forms progressively in a complex 3D pattern, which extends to the single element level.

In recent years, several groups have studied limb development at a single-cell resolution in mice,[19–23] chick,[50] and humans.[81] While all these studies characterized the cell populations during different stages of limb development, the experimental designs, tissue processing procedures, sequencing, and downstream analyses varied greatly. These differences have likely contributed to the identification of a large repertoire of limb-forming cell types. On the other hand, the different conditions used could have affected the relative proportions of these cell types. In view of that, combining the data from all these studies may provide a complete picture of the cellular composition of the developing limb.

In our work, to characterize the limb cell populations during different stages of development, we sampled cells from the entire limb daily, from E10.5 up to E14.5, using a marker-based enrichment strategy. We then utilized the obtained data to develop a model that describes the transition of limb progenitor cells into cartilage cells both temporally and spatially. Our analysis identified three progenitor populations, namely naive, proximal, and autopodial, as well as a set of marker genes for each progenitor population.

For naive progenitors, we identified a set of markers that includes *Msx1*, *Lhx2*, *Lhx9*, and *Lmo2*. Importantly, these TFs were shown to be regulated by FGF, BMP, and Shh signaling, all major pathways that regulate patterning along the three limb axes.[40–42,82–85] Using lineage studies, we validated *Msx1* as a marker for naive progenitors. This finding is in line with previous studies that suggested *Msx1* as a marker for progress zone cells.[86–90] Interestingly, we found that the naive progenitors largely maintain their transcriptional program during limb development. Finally, the finding that the pool of *Msx1* naive progenitors is maintained for several days suggests their progressive transition into proximal and autopodial progenitors.

For the proximal progenitors, we identified a set of markers that includes *Meis1* and *Meis2*, two well-known proximal markers;[17,68,69,91] *Shox2*; *Pkdcc*; and many other genes. The validity of *Shox2* as a marker for proximal cells is supported by lineage studies showing that *Shox2* lineage gives rise to the proximal part of the limb, ending at the wrist.[46]

The autopod progenitor marker set included *Hoxd13*, *Hoxa13*, and *Hoxd12*. These genes are expressed specifically in the autopod and play an essential role in digit identity and patterning.[47,48,92–96] These markers were co-expressed with *Msx1*, *Msx2*, *Lhx9*, and *Lhx2*, which were also previously shown to be important for autopod patterning,[40,42] suggesting a functional link between these two groups of genes.

The limb skeleton comprises three segments; thus, it is reasonable to assume that these segments form by three different pools of progenitors. However, in line with previous studies that failed to identify zeugopod-specific markers,[8] we could not find a zeugopod progenitor population. It is possible that the resolution of our analyses was insufficient to detect the differences between stylopod and zeugopod transcriptional programs. An alternative explanation is that while indeed there is no zeugopod-specific transcriptional program, the relative location of cells within the early limb bud determines their final fate as either stylopod or zeugopod cells, as was suggested previously by several fate mapping studies on chick.[14,97]

The identification of markers for the three progenitor populations allowed us to study their spatiotemporal distribution during limb development. We found that at E10.5–E12.5, all three progenitor cell types are present in spatially restricted domains. Proximal progenitors were initially located in the center and later expanded proximally, whereas autopodial progenitors were initially located distally in the posterior-dorsal side and later expanded anteriorly. As suggested by the single-cell results, we found that the naive progenitor marker *Msx1* was expressed throughout the process in an arc-like pattern along the AP axis, as well as dorsally and ventrally away from the AER. This finding suggests that the naive progenitors maintain their location through development. Moreover, it suggests that their progressive transition to the different lineages may not be restricted to the limb apex but can occur along the AP axis. Indeed,

Figure 6. *Msx1* lineage tracing identifies that the patterning of skeletal element deviates from the PD model

(A–X) *Msx1*$^{+}$ cells were marked at consecutive days from E9.5 to E12.5 by administration of single doses of tamoxifen to *Msx1-CreER*^{T2}*;Rosa26-tdTomato* pregnant females. Then, E13.5 whole-mount forelimbs stained with anti-SOX9 antibody (gray) were imaged by light sheet microcopy (pink, *Msx1* lineage).

(A–D) Dorsal view of 3D-rendered images showing descendants of *Msx1*$^{+}$ cells pulsed at E9.5 (A; n = 4), E10.5 (B; n = 4), E11.5 (C; n = 3), and E12.5 (D; n = 2).

(E–N) Ventral (E and J), dorsal (F and K), posterior (G and L), and anterior (H and M) views of 3D-rendered humerus images, following pulsing at E10.5 in (E)–(I‴) and at E11.5 in (J)–(N‴). The locations of optical sections shown in (I')–(I‴) and (N')–(N‴) are indicated in (I) and (N).

(O–X) Ventral (O and T), dorsal (P and U), posterior (Q and V), and anterior (R and W) views of 3D-rendered radius images, following pulsing at E10.5 in (O)–(S‴) and at E11.5 in (T)–(X‴). The locations of optical sections shown in (S')–(S‴) and (X')–(X‴) are indicated in (S) and (X).

(Y and Z) Schematics showing the spatiotemporal differentiation sequence in the forelimb skeleton from a ventral (Y) and dorsal (Z) view.

Abbreviations are as follows: Ac, acromion; R, radius; H, humerus; DT, deltoid tuberosity; HD, humeral head; LEp, lateral epicondyle; MEp, medial epicondyle; S, shaft; Pr, proximal; Ds, distal; A, anterior; P, posterior; Vn, ventral; D, dorsal; and g, gavage.

See also Figure S7.

Please cite this article in press as: Markman et al., A single-cell census of mouse limb development identifies complex spatiotemporal dynamics of skeleton formation, Developmental Cell (2023), https://doi.org/10.1016/j.devcel.2023.02.013

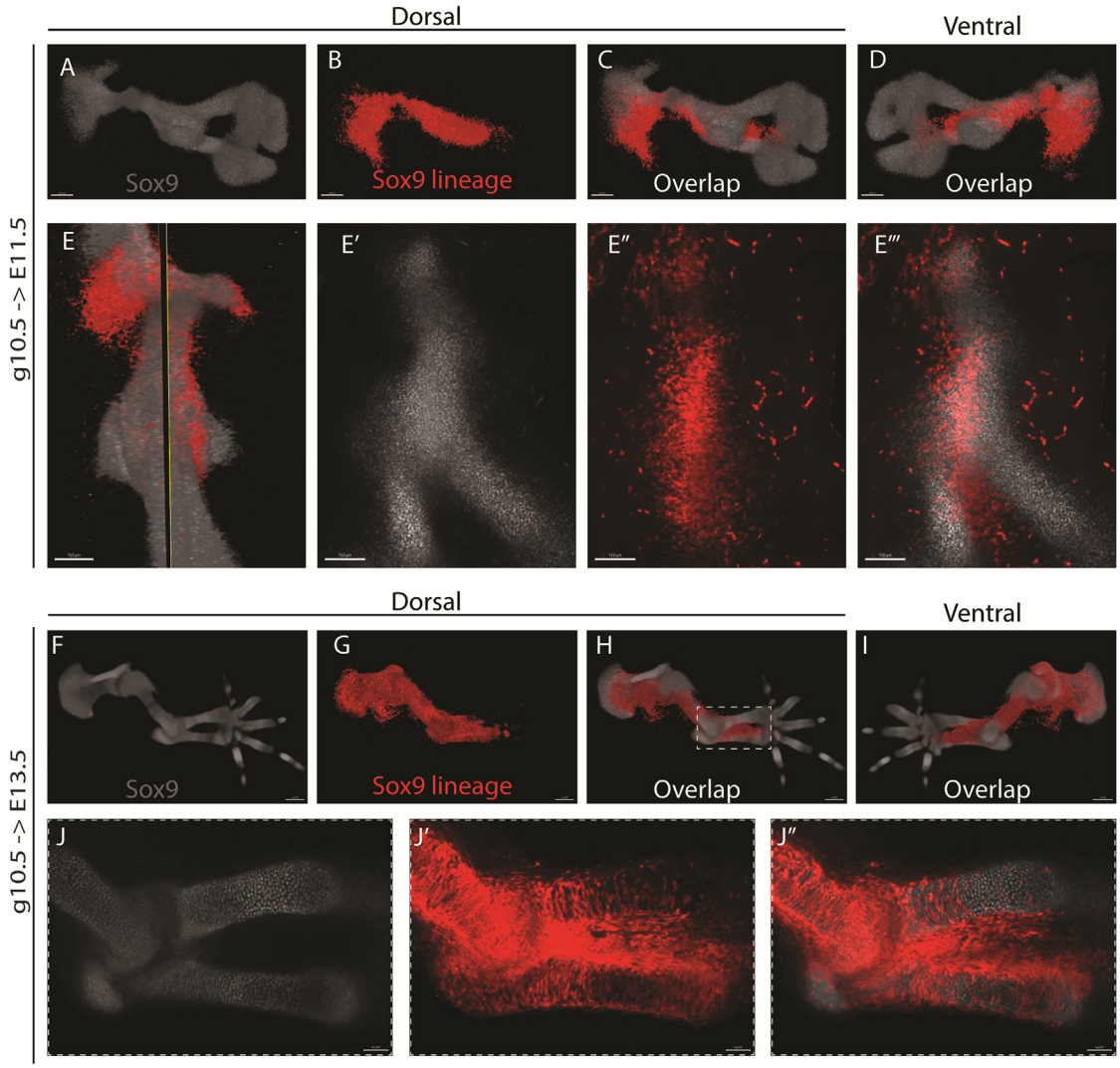

Figure 7. *Sox9* lineage tracing confirms that skeletal chondroprogenitor differentiation occurs progressively in a complex 3D pattern

(A–E‴) 3D-rendered images of *Sox9-CreER^{T2};Rosa26-tdTomato* mouse forelimbs labeled by tamoxifen administration at E10.5 and harvested 30 h later. Forelimbs were stained for *Sox9* (gray) mRNA, using *in situ* HCR, and imaged by light sheet microscopy. The locations of optical sections shown in (E')–(E‴) are indicated in (E).

(F–I) 3D-rendered images of *Sox9-CreER^{T2};Rosa26-tdTomato* mouse forelimbs labeled by tamoxifen administration at E10.5 and harvested 72 h later. Forelimbs were stained for SOX9 protein (gray) and imaged by light sheet microscopy.

(J–J″) Optical section through zeugopod segment (demarcated by dashed white square in H).

sequential pulse-chase experiments clearly showed that between E9.5 and E11.5, *Msx1* lineage cells populated extensive areas in the proximal side of the limb. Moreover, they overlapped with both proximal and autopodial progenitors. We therefore suggest that the progressive transition of naive progenitors into proximal and autopodial fates occurs along the length of the limb, allowing simultaneous transition into these identities.

As mentioned, previous mapping studies on chick limbs showed correlation between the initial location of cells and their final contribution.[14,97,98] These findings suggest that the initial position of *Msx1*$^{+}$ naive progenitors within the limb may influence their final fate. Unfortunately, the genetic approach that we applied did not provide the spatial resolution to test this hypothesis directly. Several potential mechanisms can underlie this correlation. First, simple preservation of the original spatial order may account, at least in part, for the ultimate organization. Second, the distribution and activity of molecular signals that regulate the fate of limb-forming cells may be position dependent.[6] Finally, local differences in the mechanical landscape may also affect cell fate decisions, as was suggested before.[99]

Our findings correspond with some aspects of previously suggested models of limb development. The existence of naive limb progenitors and their progressive transition into progenitors of the different limb segments were suggested by the progress zone model.[11–13] The coexistence of the different progenitors of these segments was suggested by the early specification model, whereas the progressive and concurrent specification of proximal and distal fates is consistent with the two-signal model.[16–18]

The establishment of limb progenitor identities and their differentiation to chondroprogenitors can follow two scenarios. One possibility is that the two processes are separated temporally, such that differentiation starts only after all progenitor identities have been established. Alternatively, a progressive process of identity establishment may coincide with the differentiation of the two progenitor pools into chondroprogenitors. Our findings indicate that the differentiation of naive *Msx1*$^{+}$ progenitors into chondroprogenitors is progressive and that the transition of these naive progenitors into proximal and autopodial progenitors coincides with the differentiation of these two progenitor pools into chondroprogenitors, suggesting that these processes overlap temporally. Strong support for this possibility is our observation that at E10.5–E11.5, both *Msx1*, which marks the naive progenitors, and *Sox9*, which marks chondroprogenitors, were expressed in the developing limb. Other pieces of evidence that are consistent with this scenario came from genetic lineage tracing analyses in mice. We previously showed that different skeletal elements form progressively by continuous addition of *Sox9*$^{+}$ cells.[55,100]

In this work, we provide several pieces of evidence to support the conclusion that *Msx1* is a marker for the naive mesenchymal progenitors. These include the results of our single-cell analysis and lineage tracing using *Msx1-CreER*^{T2} mice. This knockin allele was previously shown to drive an identical pattern of Cre expression as the endogenous *Msx1* gene.[79] The combination of a reliable marker mouse line and the finding that *Msx1* expression by naive mesenchymal progenitors is lost once they differentiate provided us with a unique opportunity to study the order by which the skeleton forms. If the common view is correct, and the skeleton forms in a proximal-to-distal direction, then progenitors of the proximal stylopod should be the first to lose *Msx1* expression and differentiate, followed by zeugopod progenitors, and lastly, by autopod progenitors. However, the pattern that we observed was much more complex and non-consecutive, as skeletogenesis occurred simultaneously, progressing from multiple foci along the limb. This finding indicates that in addition to the formation of skeletal elements along the PD axis, there is also strong contribution along the AP and DV axes. An example of the complexity of the process is our finding that the posterior half of the humerus formed first together with ulna, whereas the anterior side of the humerus formed later together with the radius. Further support for this notion is the similar results we obtained studying the order by which the skeleton forms, using the spatiotemporal elevation of *Sox9* expression in chondroprogenitors.

In summary, our findings suggest an alternative model for limb and skeleton development. At its core is the principle that limb development involves progressive and simultaneous transition of naive limb progenitors into either proximal or autopodial progenitors, which then progressively differentiate into *Sox9*$^{+}$ chondroprogenitors. This process occurs simultaneously at different locations along the limb, suggesting that the skeleton forms progressively from multiple foci in a complex 3D pattern.

Limitations of the study

In this work, we used single-cell RNA sequencing to identify three types of limb mesenchymal progenitors: proximal, autopodial, and naive. While we established *Msx1* as a marker gene for the naive progenitors, it is important to note that *Msx1* is not a key regulator of the naive state. Additionally, our analysis was restricted to E10.5–E14.5, thus lacking transcriptional characterization of limb mesenchyme at the onset of limb development (E9.5). This information may provide a better understanding of the key genes that are required to establish and maintain the naive state.

STAR★METHODS

Detailed methods are provided in the online version of this paper and include the following:

- KEY RESOURCES TABLE
- RESOURCE AVAILABILITY
  - Lead contact
  - Materials availability
  - Data and code availability
- EXPERIMENTAL MODEL AND SUBJECT DETAILS
  - Mouse lines
- METHOD DETAILS
  - Cell isolation and flow cytometry
  - Massively parallel single-cell RNA sequencing (MARS-Seq)
  - PACT clearing
  - Whole-mount immunostaining
  - Whole-mount *in situ* hybridization chain reaction (HCR)
  - Light-sheet fluorescence microscopy
- QUANTIFICATION AND STATISTICAL ANALYSIS
  - Low-level processing and filtering
  - Metacells modeling
  - Defining progenitor gene module signatures and scores
  - Calculation of a chondrogenic score
  - Slingshot analysis
  - Statistical analyses

SUPPLEMENTAL INFORMATION

Supplemental information can be found online at https://doi.org/10.1016/j.devcel.2023.02.013.

ACKNOWLEDGMENTS

We thank Nitzan Konstantin for expert editorial assistance; Neria Sharabi from the Department of Veterinary Resources, Weizmann Institute for his help with mouse maintenance; Dr. Yoseph Addadi and Ofra Golani from the MICC Cell Observatory unitat Life Sciences Core Facilities, Weizmann Institute, for their guidance and assistance with light sheet imaging experiments and analyses; and Dr. Tomer Meir Salame from the flow cytometry unit at Life Sciences Core Facilities, Weizmann Institute, for his assistance with FACS. We thank Efrat Davidson from the Weizmann Institute Department of Design, Photography, and Printing for designing the graphic model. Special thanks to all members of the Zelzer and Amit laboratories for encouragement and advice. I.A. is an Eden and Steven Romick Professorial Chair, supported by the Merck KGaA, Darmstadt, Germany; the Chan Zuckerberg Initiative (CZI); the HHMI International Scholar award; the European Research Council Consolidator Grant (ERC-COG) 724471-HemTree2.0; an SCA award of the Wolfson Foundation and Family Charitable Trust; the Thompson Family Foundation; an MRA Established Investigator Award (509044); the Helen and Martin Kimmel award for innovative investigation; and the NeuroMac DFG/Transregional Collaborative Research Center Grant.

This study was supported by grants from the David and Fela Shapell Family Center for Genetic Disorders and by The Estate of Mr. and Mrs. van Adelsbergen (to E.Z.).

AUTHOR CONTRIBUTIONS

S.M. designed, performed, and analyzed experiments; performed flow cytometry sorting experiments; annotated and interpreted the single-cell data; and performed and analyzed imaging experiments. M.Z. performed flow cytometry sorting experiments and library preparations. E.D. and A.G. performed single-cell bioinformatics analyses. S.M., M.Z., E.D., A.G., I.A., and E.Z. generated the figures. S.M., E.Z., and I.A. wrote the manuscript. E.Z. and I.A. supervised the project. All authors discussed the results and commented on the manuscript at all stages.

DECLARATION OF INTERESTS

The authors declare no competing interests.

Received: January 17, 2022
Revised: October 20, 2022
Accepted: February 20, 2023
Published: March 16, 2023

REFERENCES

1. Johnson, R.L., and Tabin, C.J. (1997). Molecular models for vertebrate-limbdevelopment. Cell *90*, 979–990. https://doi.org/10.1016/S0092-8674(00)80364-5.
2. Niswander, L. (2003). Pattern formation: old models out on a limb. Nat. Rev. Genet. *4*, 133–143. https://doi.org/10.1038/NRG1001.
3. Tickle, C. (2005). Making digit patterns in the vertebrate limb. Nat. Rev. Mol. Cell Biol. *7*, 45–53. https://doi.org/10.1038/NRM1830.
4. Zuniga, A. (2015). Next generation limb development and evolution: old questions, new perspectives. Development *142*, 3810–3820. https://doi.org/10.1242/DEV.125757.
5. Huang, A.H. (2017). Coordinated development of the limb musculoskeletal system: tendon and muscle patterning and integration with the skeleton. Dev. Biol. *429*, 420–428. https://doi.org/10.1016/J.YDBIO.2017.03.028.
6. Delgado, I., and Torres, M. (2017). Coordination of limb development by crosstalk among axial patterning pathways. Dev. Biol. *429*, 382–386. https://doi.org/10.1016/J.YDBIO.2017.03.006.
7. Nassari, S., Duprez, D., and Fournier-Thibault, C. (2017). Non-myogenic contribution to muscledevelopment and homeostasis: therole of connectivetissues. Front. Cell Dev. Biol. *5*, 22. https://doi.org/10.3389/FCELL.2017.00022.
8. Tabin, C., and Wolpert, L. (2007). Rethinking the proximodistal axis of the vertebrate limb in the molecular era. Genes Dev. *21*, 1433–1442. https://doi.org/10.1101/GAD.1547407.
9. Zeller, R., López-Ríos, J., and Zuniga, A. (2009). Vertebrate limb bud development: moving towards integrative analysis of organogenesis. Nat. Rev. Genet. *10*, 845–858. https://doi.org/10.1038/nrg2681.
10. Petit, F., Sears, K.E., and Ahituv, N. (2017). Limb development: a paradigm of gene regulation. Nat. Rev. Genet. *18*, 245–258. https://doi.org/10.1038/NRG.2016.167.
11. Saunders, J.W. (1948). The proximo-distal sequence of origin of the parts of the chick wing and the role of the ectoderm. J. Exp. Zool. *108*, 363–403. https://doi.org/10.1002/jez.1401080304.
12. Summerbell, D., Lewis, J.H., and Wolpert, L. (1973). Positional information in chicklimbmorphogenesis. Nature *244*, 492–496. https://doi.org/10.1038/244492a0.
13. Wolpert, L. (2002). The progress zone model for specifying positional information. Int. J. Dev. Biol. *46*, 869–870. https://doi.org/10.1387/IJDB.12455622.
14. Dudley, A.T., Ros, M.A., and Tabin, C.J. (2002). A re-examination of proximodistal patterning during vertebrate limb development. Nature *418*, 539–544. https://doi.org/10.1038/nature00945.
15. Sun, X., Mariani, F.V., and Martin, G.R. (2002). Functions of FGF signalling from the apical ectodermal ridge in limb development. Nature *418*, 501–508. https://doi.org/10.1038/nature00902.
16. Mercader, N., Leonardo, E., Piedra, M.E., Martínez-A, C., Ros, M.A., and Torres, M. (2000). Opposing RA and FGF signals control proximodistal vertebrate limb development through regulation of Meis genes. Development *127*, 3961–3970.
17. Mercader, N., Leonardo, E., Azplazu, N., Serrano, A., Morata, G., Martínez, C., and Torres, M. (1999). Conserved regulation of proximodistal limb axis development by Meis1/Hth. Nature *402*, 425–429. https://doi.org/10.1038/46580.
18. Mariani, F.V., Ahn, C.P., and Martin, G.R. (2008). Genetic evidence that FGFs play an instructive role in limb proximal-distal patterning. Nature *453*, 401–405. https://doi.org/10.1038/NATURE06876.
19. Bastide, S., Chomsky, E., Saudemont, B., Loe-Mie, Y., Schmutz, S., Novault, S., Marlow, H., Tanay, A., and Spitz, F. (2022). TATTOO-seq delineates spatial and cell type-specific regulatory programs during limb patterning. https://doi.org/10.1101/2022.03.20.482385.
20. Cao, J., Spielmann, M., Qiu, X., Huang, X., Ibrahim, D.M., Hill, A.J., Zhang, F., Mundlos, S., Christiansen, L., Steemers, F.J., et al. (2019). The single-cell transcriptional landscape of mammalian organogenesis. Nature *566*, 496–502. https://doi.org/10.1038/s41586-019-0969-x.
21. Desanlis, I., Paul, R., and Kmita, M. (2020). Transcriptional trajectories in mouselimbbudsreveal the transition from anterior-posterior to proximal-distalpatterning at earlylimbbudstage. J. Dev. Biol. *8*, 1–16. https://doi.org/10.3390/JDB8040031.
22. He, P., Williams, B.A., Trout, D., Marinov, G.K., Amrhein, H., Berghella, L., Goh, S.T., Plajzer-Frick, I., Afzal, V., Pennacchio, L.A., et al. (2020). The changing mouse embryo transcriptome at whole tissue and single-cell resolution. Nature *583*, 760–767. https://doi.org/10.1038/s41586-020-2536-x.
23. Kelly, N.H., Huynh, N.P.T., and Guilak, F. (2020). Single cell RNA-sequencing reveals cellular heterogeneity and trajectories of lineage specification during murine embryonic limb development. Matrix Biol. *89*, 1–10. https://doi.org/10.1016/J.MATBIO.2019.12.004.
24. Bi, W., Deng, J.M., Zhang, Z., Behringer, R.R., and de Crombrugghe, B. (1999). Sox9 is required for cartilage formation. Nat. Genet. *22*, 85–89.
25. Akiyama, H., Chaboissier, M.C., Martin, J.F., Schedl, A., and de Crombrugghe, B. (2002). The transcription factor Sox9 has essential roles in successive steps of the chondrocyte differentiation pathway and is required for expression of Sox5 and Sox6. Genes Dev. *16*, 2813–2828. https://doi.org/10.1101/GAD.1017802.
26. Schweitzer, R., Chyung, J.H., Murtaugh, L.C., Brent, A.E., Rosen, V., Olson, E.N., Lassar, A., and Tabin, C.J. (2001). Analysis of the tendon cell fate using scleraxis, a specific marker for tendons and ligaments. Development *128*, 3855–3866.
27. Akiyama, H., Kim, J.-E., Nakashima, K., Balmes, G., Iwai, N., Deng, J.M., Zhang, Z., Martin, J.F., Behringer, R.R., Nakamura, T., and de Crombrugghe, B. (2005). Osteo-chondroprogenitor cells are derived from Sox9 expressing precursors. Proc. Natl. Acad. Sci. USA *102*, 14665–14670. https://doi.org/10.1073/PNAS.0504750102.
28. Soeda, T., Deng, J.M., de Crombrugghe, B., Behringer, R.R., Nakamura, T., and Akiyama, H. (2010). Sox9-expressing precursors are the cellular origin of the cruciate ligament of the knee joint and the limb tendons. Genesis *48*, 635–644. https://doi.org/10.1002/dvg.20667.
29. Sugimoto, Y., Takimoto, A., Akiyama, H., Kist, R., Scherer, G., Nakamura, T., Hiraki, Y., and Shukunami, C. (2013). Scx+/Sox9+ progenitors contribute to the establishment of the junction between cartilage and tendon/ligament. Development *140*, 2280–2288. https://doi.org/10.1242/dev.096354.
30. Nagakura, R., Yamamoto, M., Jeong, J., Hinata, N., Katori, Y., Chang, W.J., and Abe, S. (2020). Switching of Sox9 expression during musculoskeletal system development. Sci. Rep. *10*, 8425.

31. Madisen, L., Zwingman, T.A., Sunkin, S.M., Oh, S.W., Zariwala, H.A., Gu, H., Ng, L.L., Palmiter, R.D., Hawrylycz, M.J., Jones, A.R., et al. (2010). A robust and high-throughput Cre reporting and characterization system for the whole mouse brain. Nat. Neurosci. *13*, 133–140. https://doi.org/10.1038/nn.2467.

32. Pryce, B.A., Brent, A.E., Murchison, N.D., Tabin, C.J., and Schweitzer, R. (2007). Generation of transgenic tendon reporters, ScxGFP and ScxAP, using regulatory elements of the scleraxis gene. Dev. Dyn. *236*, 1677–1682. https://doi.org/10.1002/dvdy.21179.

33. Baran, Y., Bercovich, A., Sebe-Pedros, A., Lubling, Y., Giladi, A., Chomsky, E., Meir, Z., Hoichman, M., Lifshitz, A., and Tanay, A. (2019). MetaCell: analysis of single-cellRNA-seqdata using K-nn graph partitions. Genome Biol. *20*, 206. https://doi.org/10.1186/s13059-019-1812-2.

34. Bell, D.M., Leung, K.K.H., Wheatley, S.C., Ng, L.J., Zhou, S., Ling, K.W., Sham, M.H., Koopman, P., Tam, P.P.L., and Cheah, K.S.E. (1997). SOX9 directly regulates the type-II collagen gene. Nat. Genet. *16*, 174–178. https://doi.org/10.1038/ng0697-174.

35. Lefebvre, V.R., Huang, W., Harley, V.R., Goodfellow, P.N., and De Crombrugghe, B. (1997). SOX9 is a potentactivator of the chondrocyte-specificenhancer of the pro alpha1(II) collagen gene of the proalpha1(II) collagen gene. Mol. Cell. Biol. *17*, 2336–2346.

36. Nakamura, Y., Yamamoto, K., He, X., Otsuki, B., Kim, Y., Murao, H., Soeda, T., Tsumaki, N., Deng, J.M., Zhang, Z., et al. (2011). Wwp2 is essential for palatogenesis mediated by the interaction between Sox9 and mediator subunit 25. Nat. Commun. *2*, 251. https://doi.org/10.1038/ncomms1242.

37. Stricker, S., Mathia, S., Haupt, J., Seemann, P., Meier, J., and Mundlos, S. (2012). Odd-skippedrelatedgenesregulatedifferentiation of embryoniclimb-mesenchyme and bonemarrowmesenchymalstromalcells. StemCells Dev. *21*, 623–633. https://doi.org/10.1089/scd.2011.0154.

38. Vallecillo-García, P., Orgeur, M., Vom Hofe-Schneider, S., Stumm, J., Kappert, V., Ibrahim, D.M., Börno, S.T., Hayashi, S., Relaix, F., Hildebrandt, K., et al. (2017). Odd skipped-related 1 identifies a population of embryonic fibro-adipogenic progenitors regulating myogenesis during limb development. Nat. Commun. *8*, 1218. https://doi.org/10.1038/s41467-017-01120-3.

39. Liu, H., Xu, J., Liu, C.F., Lan, Y., Wylie, C., and Jiang, R. (2015). Whole transcriptome expression profiling of mouse limb tendon development by using RNA-seq. J. Orthop. Res. *33*, 840–848. https://doi.org/10.1002/JOR.22886.

40. Lallemand, Y., Nicola, M.A., Ramos, C., Bach, A., Cloment, C.S., and Robert, B. (2005). Analysis of Msx1; Msx2 double mutants reveals multiple roles for Msx genes in limb development. Development *132*, 3003–3014. https://doi.org/10.1242/DEV.01877.

41. Bensoussan-Trigano, V., Lallemand, Y., Saint Cloment, C., and Robert, B. (2011). Msx1 and Msx2 in limb mesenchyme modulate digit number and identity. Dev. Dyn. *240*, 1190–1202. https://doi.org/10.1002/DVDY.22619.

42. Tzchori, I., Day, T.F., Carolan, P.J., Zhao, Y., Wassif, C.A., Li, L., Lewandoski, M., Gorivodsky, M., Love, P.E., Porter, F.D., et al. (2009). LIM homeobox transcription factors integrate signaling events that control three-dimensional limb patterning and growth. Development *136*, 1375–1385. https://doi.org/10.1242/DEV.026476.

43. Zhou, X., Benson, K.F., Ashar, H.R., and Chada, K. (1995). Mutation responsible for the mouse pygmy phenotype in the developmentally regulated factor HMGI-C. Nature *376*, 771–774.

44. Hirning-Folz, U., Wilda, M., Rippe, V., Bullerdiek, J., and Hameister, H. (1998). The expression pattern of the Hmgic gene during development. Genes Chromosomes Cancer *23*, 350–357.

45. Salbaum, J.M. (1998). Punc, a novel mouse gene of the immunoglobulin-superfamily, is expressed predominantly in the developing nervous system. Mech. Dev. *71*, 201–204. https://doi.org/10.1016/S0925-4773(98)00005-7.

46. Sun, C., Zhang, T., Liu, C., Gu, S., and Chen, Y. (2013). Generation of Shox2-Cre allele for tissue specific manipulation of genes in the developing heart, palate, and limb. Genesis *51*, 515–522. https://doi.org/10.1002/DVG.22397.

47. Scotti, M., Kherdjemil, Y., Roux, M., and Kmita, M. (2015). A Hoxa13: Cre mousestrain for conditionalgenemanipulation in developinglimb, hindgut, and urogenitalsystem. Genesis *53*, 366–376. https://doi.org/10.1002/DVG.22859.

48. Fromental-Ramain, C., Warot, X., Messadecq, N., LeMeur, M., Dollé, P., and Chambon, P. (1996). Hoxa-13 and Hoxd-13 play a crucial role in the patterning of the limb autopod. Development *122*, 2997–3011. https://doi.org/10.1242/DEV.122.10.2997.

49. Kult, S., Olender, T., Osterwalder, M., Markman, S., Leshkowitz, D., Krief, S., Blecher-Gonen, R., Ben-Moshe, S., Farack, L., Keren-Shaul, H., et al. (2021). Bi-fated tendon-to-bone attachmentcells are regulated by shared enhancers and KLF transcription factors. eLife *10*, 1–29. https://doi.org/10.7554/eLife.55361.

50. Feregrino, C., Sacher, F., Parnas, O., and Tschopp, P. (2019). A single-cell transcriptomic atlas of the developing chicken limb. BMC Genomics *20*, 401. https://doi.org/10.1186/S12864-019-5802-2.

51. Gehwolf, R., Wagner, A., Lehner, C., Bradshaw, A.D., Scharler, C., Niestrawska, J.A., Holzapfel, G.A., Bauer, H.C., Tempfer, H., and Traweger, A. (2016). Pleiotropic roles of the matricellular protein Sparc in tendon maturation and ageing. Sci. Rep. *61*, 32635. https://doi.org/10.1038/srep32635.

52. Kou, I., and Ikegawa, S. (2004). SOX9-dependent and -independent transcriptional regulation of human cartilage link protein. J. Biol. Chem. *279*, 50942–50948. https://doi.org/10.1074/jbc.M406786200.

53. Watanabe, H., and Yamada, Y. (1999). Mice lacking link protein develop dwarfism and craniofacial abnormalities. Nat. Genet. *21*, 225–229.

54. Han, M.S., Kim, J.E., Shin, H.I., and Kim, I.S. (2008). Expression patterns of βig-h3 in chondrocyte differentiation during endochondral ossification. Exp. Mol. Med. *40*, 453–460. https://doi.org/10.3858/emm.2008.40.4.453.

55. Blitz, E., Sharir, A., Akiyama, H., and Zelzer, E. (2013). Tendon-bone attachment unit is formed modularly by a distinct pool of *Scx* – and *Sox9* -positive progenitors. Development *140*, 2680–2690. https://doi.org/10.1242/dev.093906.

56. Shen, H., Wilke, T., Ashique, A.M., Narvey, M., Zerucha, T., Savino, E., Williams, T., and Richman, J.M. (1997). Chicken transcription factor AP-2: cloning, expression and itsrole in outgrowth of facialprominences and limbbuds. Dev. Biol. *188*, 248–266. https://doi.org/10.1006/DBIO.1997.8617.

57. Zhao, F., Bosserhoff, A.K., Buettner, R., and Moser, M. (2011). A heart-hand syndromegene: Tfap2b plays a criticalrole in the development and remodeling of mouseductusarteriosus and limbpatterning. PLoS One *6*, e22908. https://doi.org/10.1371/JOURNAL.PONE.0022908.

58. Wang, J., Rao, S., Chu, J., Shen, X., Levasseur, D.N., Theunissen, T.W., and Orkin, S.H. (2006). A protein interaction network for pluripotency of embryonic stem cells. Nature *444*, 364–368. https://doi.org/10.1038/nature05284.

59. Zhang, J., Tam, W.L., Tong, G.Q., Wu, Q., Chan, H.Y., Soh, B.S., Lou, Y., Yang, J., Ma, Y., Chai, L., et al. (2006). Sall4 modulates embryonic stem cell pluripotency and early embryonic development by the transcriptional regulation of Pou5f1. Nat. Cell Biol. *8*, 1114–1123. https://doi.org/10.1038/ncb1481.

60. Zhang, J., Ratanasirintrawoot, S., Chandrasekaran, S., Wu, Z., Ficarro, S.B., Yu, C., Ross, C.A., Cacchiarelli, D., Xia, Q., Seligson, M., et al. (2016). LIN28 regulatesstem cellmetabolism and conversion to primed-pluripotency. Cell StemCell *19*, 66–80. https://doi.org/10.1016/j.stem.2016.05.009.

61. Yu, J., Vodyanik, M.A., Smuga-Otto, K., Antosiewicz-Bourget, J., Frane, J.L., Tian, S., Nie, J., Jonsdottir, G.A., Ruotti, V., Stewart, R., et al. (2007). Induced pluripotentstem celllinesderived from humansomaticcells. Science *318*, 1917–1920. https://doi.org/10.1126/SCIENCE.1151526.

62. Patterson, M., Chan, D.N., Ha, I., Case, D., Cui, Y., Van Handel, B., Mikkola, H.K., and Lowry, W.E. (2011). Defining the nature of human pluripotent stem cell progeny. Cell Res. *22*, 178–193. https://doi.org/10.1038/cr.2011.133.

63. Pastor, W.A., Liu, W., Chen, D., Ho, J., Kim, R., Hunt, T.J., Lukianchikov, A., Liu, X., Polo, J.M., Jacobsen, S.E., and Clark, A.T. (2018). TFAP2C regulates transcription in human naive pluripotency by opening enhancers. Nat. Cell Biol. *20*, 553–564. https://doi.org/10.1038/s41556-018-0089-0.

64. Melton, C., Judson, R.L., and Blelloch, R. (2010). Opposing microRNA families regulate self-renewal in mouse embryonic stem cells. Nature *463*, 621–626. https://doi.org/10.1038/nature08725.

65. Worringer, K.A., Rand, T.A., Hayashi, Y., Sami, S., Takahashi, K., Tanabe, K., Narita, M., Srivastava, D., and Yamanaka, S. (2014). The let-7/LIN-41 pathwayregulatesreprogramming to humaninducedpluripotentstem cells by controllingexpression of prodifferentiation genes. Cell StemCell *14*, 40–52. https://doi.org/10.1016/J.STEM.2013.11.001.

66. Chang, H.-M., Martinez, N.J., Thornton, J.E., Hagan, J.P., Nguyen, K.D., and Gregory, R.I. (2012). Trim71 cooperates with microRNAs to repress Cdkn1a expression and promote embryonic stem cell proliferation. Nat. Commun. *31*, 923. https://doi.org/10.1038/ncomms1909.

67. Rybak, A., Fuchs, H., Hadian, K., Smirnova, L., Wulczyn, E.A., Michel, G., Nitsch, R., Krappmann, D., and Wulczyn, F.G. (2009). The let-7 target gene mouse lin-41 is a stem cell specific E3 ubiquitin ligase for the miRNApathway protein Ago2. Nat. Cell Biol. *11*, 1411–1420. https://doi.org/10.1038/ncb1987.

68. Mercader, N., Selleri, L., Criado, L.M., Pallares, P., Parras, C., Cleary, M.L., and Torres, M. (2009). Ectopic Meis1 expression in the mouse limb bud alters P-D patterning in a Pbx1-independent manner. Int. J. Dev. Biol. *53*, 1483–1494. https://doi.org/10.1387/IJDB.072430NM.

69. Delgado, I., López-Delgado, A.C., Roselló-Díez, A., Giovinazzo, G., Cadenas, V., Fernández-de-Manuel, L., Sánchez-Cabo, F., Anderson, M.J., Lewandoski, M., and Torres, M. (2020). Proximo-distal positional information encoded by an Fgf-regulated gradient of homeodomaintranscription factors in the vertebrate limb. Sci. Adv. *6*, eaaz0742. https://doi.org/10.1126/SCIADV.AAZ0742.

70. Probst, S., Kraemer, C., Demougin, P., Sheth, R., Martin, G.R., Shiratori, H., Hamada, H., Iber, D., Zeller, R., and Zuniga, A. (2011). SHH propagates distal limb bud development by enhancing CYP26B1-mediated retinoic acid clearance via AER-FGF signalling. Development *138*, 1913–1923. https://doi.org/10.1242/DEV.063966.

71. Vickerman, L., Neufeld, S., and Cobb, J. (2011). Shox2 function couples neural, muscular and skeletal development in the proximal forelimb. Dev. Biol *350*, 323–336. https://doi.org/10.1016/j.ydbio.2010.11.031.

72. Reijntjes, S., Stricker, S., and Mankoo, B.S. (2007). A comparative analysis of Meox1 and Meox2 in the developing somites and limbs of the chick embryo. Int. J. Dev. Biol. *51*, 753–759. https://doi.org/10.1387/ijdb.072332sr.

73. Campbell, A.L., Shih, H.P., Xu, J., Gross, M.K., and Kioussi, C. (2012). Regulation of motility of myogeniccells in fillinglimbmuscleanlagen by Pitx2. PLoS One *7*, e35822. https://doi.org/10.1371/JOURNAL.PONE.0035822.

74. Pellegrini, M., Pantano, S., Fumi, M.P., Lucchini, F., and Forabosco, A. (2001). Agenesis of the scapula in Emx2 homozygousmutants. Dev. Biol. *232*, 149–156. https://doi.org/10.1006/DBIO.2001.0159.

75. Li, D., Sakuma, R., Vakili, N.A., Mo, R., Puviindran, V., Deimling, S., Zhang, X., Hopyan, S., and Hui, C.C. (2014). Formation of proximal and anterior limb skeleton requires early function of Irx3 and Irx5 and is negatively regulated by Shh signaling. Dev. Cell *29*, 233–240. https://doi.org/10.1016/J.DEVCEL.2014.03.001.

76. Wilson-Rawls, J., Rhee, J.M., and Rawls, A. (2004). Paraxis is a basic Helix-Loop-Helix proteinthatpositivelyregulatestranscription through binding to specific E-box elements. J. Biol. Chem. *279*, 37685–37692. https://doi.org/10.1074/jbc.M401319200.

77. Nassari, S., Blavet, C., Bonnin, M.A., Stricker, S., Duprez, D., and Fournier-Thibault, C. (2017). The chemokines CXCL12 and CXCL14 differentially regulate connective tissue markers during limb development. Sci. Rep. *7*, 17279. https://doi.org/10.1038/s41598-017-17490-z.

78. Coudert, A.E., Pibouin, L., Vi-Fane, B., Thomas, B.L., Macdougall, M., Choudhury, A., Robert, B., Sharpe, P.T., Berdal, A., and Lezot, F. (2005). Expression and regulation of the Msx1 natural antisense transcript during development. Nucleic Acids Res. *33*, 5208–5218. https://doi.org/10.1093/NAR/GKI831.

79. Lallemand, Y., Moreau, J., Cloment, C.S., Vives, F.L., and Robert, B. (2013). Generation and characterization of a tamoxifen inducible Msx1CreERT2 knock-in allele. Genesis *51*, 110–119. https://doi.org/10.1002/DVG.22350.

80. de Crombrugghe, B., Lefebvre, V., Behringer, R.R., Bi, W., Murakami, S., and Huang, W. (2000). Transcriptional mechanisms of chondrocyte differentiation. Matrix Biol. *19*, 389–394.

81. Zhang, B., He, P., Lawrence, J.E., Wang, S., Tuck, E., Williams, B., Roberts, K., Kleshchevnikov, V., Mamanova, L., Bolt, L., et al. (2022). A human embryonic limb cell atlas resolved in space and time. https://doi.org/10.1101/2022.04.27.489800.

82. Lallemand, Y., Bensoussan, V., Cloment, C.S., and Robert, B. (2009). Msx genes are important apoptosis effectors downstream of the Shh/Gli3 pathway in the limb. Dev. Biol. *331*, 189–198. https://doi.org/10.1016/J.YDBIO.2009.04.038.

83. Alappat, S., Zhang, Z.Y., and Chen, Y.P. (2003). Msx homeobox gene family and craniofacial development. Cell Res. *13*, 429–442. https://doi.org/10.1038/sj.cr.7290185.

84. Watson, B.A., Feenstra, J.M., Van Arsdale, J.M., Rai-Bhatti, K.S., Kim, D.J.H., Coggins, A.S., Mattison, G.L., Yoo, S., Steinman, E.D., Pira, C.U., et al. (2018). LHX2 mediates the FGF-to-SHH regulatoryloop during limbdevelopment. J. Dev. Biol. *6*, 13. https://doi.org/10.3390/JDB6020013.

85. Yang, Y., and Wilson, M.J. (2015). Lhx9 gene expression during early limb development in mice requires the FGF signalling pathway. Gene Expr. Patterns *19*, 45–51. https://doi.org/10.1016/J.GEP.2015.07.002.

86. Davidson, D.R., Crawley, A., Hill, R.E., and Tickle, C. (1991). Position-dependent expression of two related homeobox genes in developing vertebrate limbs. Nature *352*, 429–431. https://doi.org/10.1038/352429a0.

87. Coelho, C.N.D., Krabbenhoft, K.M., Upholt, W.B., Fallon, J.F., and Kosher, R.A. (1991). Altered expression of the chicken homeobox-containing genes GHox-7 and GHox-8 in the limb buds of limbless mutant chick embryos. Development *113*, 1487–1493. https://doi.org/10.1242/DEV.113.4.1487.

88. Robert, B., Lyons, G., Simandl, B.K., Kuroiwa, A., and Buckingham, M. (1991). The apical ectodermal ridge regulates Hox-7 and Hox-8 gene expression in developing chick limb buds. Genes Dev. *5*, 2363–2374. https://doi.org/10.1101/GAD.5.12B.2363.

89. Ros, M.A., Lyons, G., Kosher, R.A., Upholt, W.B., Coelho, C.N., and Fallon, J.F. (1992). Apical ridge dependent and independent mesodermal domains of GHox-7 and GHox-8 expression in chick limb buds. Development *116*, 811–818.

90. Wang, Y., and Sassoon, D. (1995). Ectoderm-mesenchyme and mesenchyme-mesenchymeinteractionsregulate Msx-1 expression and cellular-differentiation in the murinelimbbud. Dev. Biol. *168*, 374–382. https://doi.org/10.1006/DBIO.1995.1087.

91. Capdevila, J., Tsukui, T., Rodríquez Esteban, C., Zappavigna, V., and Izpisúa Belmonte, J.C. (1999). Control of vertebratelimboutgrowth by the proximalfactor Meis2 and distalantagonism of BMPs by gremlin. Mol. Cell *4*, 839–849. https://doi.org/10.1016/S1097-2765(00)80393-7.

92. Desanlis, I., Kherdjemil, Y., Mayran, A., Bouklouch, Y., Gentile, C., Sheth, R., Zeller, R., Drouin, J., and Kmita, M. (2020). HOX13-dependent chromatin accessibility underlies the transition towards the digit development program. Nat. Commun. *11*, 2491. https://doi.org/10.1038/s41467-020-16317-2.

93. Fabre, P.J., Leleu, M., Mascrez, B., Lo Giudice, Q., Cobb, J., and Duboule, D. (2018). Heterogeneous combinatorial expression of Hoxd genes in single cells during limb development. BMC Biol. *16*, 101. https://doi.org/10.1186/S12915-018-0570-Z.

94. Zákány, J., Fromental-Ramain, C., Warot, X., and Duboule, D. (1997). Regulation of number and size of digits by posterior Hox genes: a dose-dependent mechanism with potential evolutionaryimplications. Proc. Natl. Acad. Sci. USA *94*, 13695–13700. https://doi.org/10.1073/PNAS.94.25.13695.

95. Sheth, R., Bastida, M.F., and Ros, M. (2007). Hoxd and Gli3 interactions modulate digit number in the amniote limb. Dev. Biol. *310*, 430–441. https://doi.org/10.1016/J.YDBIO.2007.07.023.

96. Knezevic, V., De Santo, R., Schughart, K., Huffstadt, U., Chiang, C., Mahon, K.A., and Mackem, S. (1997). Hoxd-12 differentially affects preaxial and postaxial chondrogenic branches in the limb and regulates Sonic hedgehog in a positive feedback loop. Development *124*, 4523–4536. https://doi.org/10.1242/DEV.124.22.4523.

97. Sato, K., Koizumi, Y., Takahashi, M., Kuroiwa, A., and Tamura, K. (2007). Specification of cell fate along the proximal-distal axis in the developing chick limb bud. Development *134*, 1397–1406. https://doi.org/10.1242/DEV.02822.

98. Vargesson, N., Clarke, J.D., Vincent, K., Coles, C., Wolpert, L., and Tickle, C. (1997). Cell fate in the chick limb bud and relationship to gene expression. Development *124*, 1909–1918. https://doi.org/10.1242/DEV.124.10.1909.

99. Zhu, M., Tao, H., Samani, M., Luo, M., Wang, X., Hopyan, S., and Sun, Y. (2018). Three-dimensional tissue stiffness mapping in the mouse embryo supports durotaxis during early limb bud morphogenesis. https://doi.org/10.1101/412072.

100. Eyal, S., Kult, S., Rubin, S., Krief, S., Felsenthal, N., Pineault, K.M., Leshkowitz, D., Salame, T.M., Addadi, Y., Wellik, D.M., et al. (2019). Bone morphology is regulated modularly by global and regional genetic programs. Development *146*, dev167882. https://doi.org/10.1242/DEV.167882/VIDEO-3.

101. Jaitin, D.A., Kenigsberg, E., Keren-Shaul, H., Elefant, N., Paul, F., Zaretsky, I., Mildner, A., Cohen, N., Jung, S., Tanay, A., and Amit, I. (2014). Massively parallel single-cellRNA-seq for marker-free decomposition of tissues into cell types. Science *343*, 776–779. https://doi.org/10.1126/science.1247651.

102. Chan, H.Y., V, S., Xing, X., Kraus, P., Yap, S.P., Ng, P., Lim, S.L., and Lufkin, T. (2011). Comparison of IRES and F2A-basedlocus-specificmulticistronicexpression in stablemouselines. PLoS One *6*, e28885. https://doi.org/10.1371/JOURNAL.PONE.0028885.

103. Treweek, J.B., Chan, K.Y., Flytzanis, N.C., Yang, B., Deverman, B.E., Greenbaum, A., Lignell, A., Xiao, C., Cai, L., Ladinsky, M.S., et al. (2015). Whole-body tissue stabilization and selective extractions via tissue-hydrogel hybrids for high-resolution intact circuit mapping and phenotyping. Nat. Protoc. *10*, 1860–1896. https://doi.org/10.1038/nprot.2015.122.

104. Yang, B., Treweek, J.B., Kulkarni, R.P., Deverman, B.E., Chen, C.K., Lubeck, E., Shah, S., Cai, L., and Gradinaru, V. (2014). Single-cellphenotyping withintransparentintacttissue through whole-bodyclearing. Cell *158*, 945–958. https://doi.org/10.1016/J.CELL.2014.07.017.

105. Kim, D., Langmead, B., and Salzberg, S.L. (2015). HISAT: a fast spliced aligner with low memory requirements. Nat. Methods *12*, 357–360. https://doi.org/10.1038/nmeth.3317.

106. Street, K., Risso, D., Fletcher, R.B., Das, D., Ngai, J., Yosef, N., Purdom, E., and Dudoit, S. (2018). Slingshot: cell lineage and pseudotime inference for single-cell transcriptomics. BMC Genomics *19*, 477. https://doi.org/10.1186/S12864-018-4772-0/FIGURES/5.

Please cite this article in press as: Markman et al., A single-cell census of mouse limb development identifies complex spatiotemporal dynamics of skeleton formation, Developmental Cell (2023), https://doi.org/10.1016/j.devcel.2023.02.013

STAR★METHODS

KEY RESOURCES TABLE

REAGENT or RESOURCE	SOURCE	IDENTIFIER
Antibodies		
Rabbit anti-SOX9	Sigma-Aldrich	AB5535; RRID: AB_2239761
Cy5 conjugated donkey anti-rabbit	Jackson Immuno Research laboratory	Cat# 711-175-152; RRID: AB_2340607
Chemicals, peptides, and recombinantproteins		
Collagenase type V	Sigma Aldrich	Cat# C9263
Histodenz	Sigma Aldrich	Cat# D2158
Low gelling agarose	Sigma Aldrich	Cat# A9414
Thermal initiator 2,2'-azobis[2-(2-imidazolin-2-yl) propane]dihydrochloride	*FUJIFILM Wako Chemical*	Cat# VA-044
Critical commercial assays		
HCR in situ reagents	Molecular Technologies	N/A
Deposited data		
Raw data files for single-cell RNA-seq	NCBI Gene Expression Omnibus	GEO: GSE185940
Experimental models: Organisms/strains		
Mouse: C57BL/6JOlaHsd	Envigo	N/A
Mouse: *Sox9-CreER*^{T2}	Haruhiko Akiyama, The University of Texas M.D. Anderson Cancer Center	N/A
Mouse: *Scx-GFP*	Ronen Schweitzer, Oregon Health and Science University	N/A
Mouse: *Msx1-CreER*^{T2}	The Jackson Laboratory	Cat# 027850
Mouse: *Rosa26-tdTomato*	The Jackson Laboratory	Cat# 007914
Software and algorithms		
R version 4.1.3	The R Foundation	http://www.r-project.org/
FlowJo software	FlowJo	https://www.flowjo.com/
Slingshot package	Bioconductor	https://bioconductor.org/packages/release/bioc/html/slingshot.html
Imaris v9.8	Imaris	N/A
Other		
MARS-seq reagents	Provided by Jaitin et al.[101]	N/A

RESOURCE AVAILABILITY

Lead contact

Further information and requests for resources and reagents should be directed to and will be fulfilled by the Lead Contact, Elazar Zelzer (Eli.zelzer@weizmann.ac.il).

Materials availability

This study did not generate new unique reagents.

Data and code availability

The accession number for the raw and processed scRNA-seqdata reported in this paper is GEO: GSE185940. Microscopy data reported in this paper will be shared by the lead contact upon request. Any additional information required to reanalyze the data reported in this paper is available from the lead contact upon request.

EXPERIMENTAL MODEL AND SUBJECT DETAILS

Mouse lines

The generation of *Sox9-CreER^{T2}*,[28] *Scx-GFP*,[32] *Msx1-CreER^{T2}*,[79] *Sox9-GFP*[102] and *Rosa26-tdTomato*[31] mice has been described previously. For fluorescence-activated cell sorting (FACS) experiments, *Sox9-CreER^{T2}-tdTomato*;*Scx-GFP* or *Sox9-GFP* mice were crossed with *Rosa26-tdTomato;Scx-GFP* or C57BL/6 mice, respectively. For lineage tracing experiments, *Msx1-CreER^{T2}* were crossed with *Rosa26-tdTomato* or with *Rosa26-tdTomato;Scx-GFP* reporter mice.

Induction of Cre recombinase was performed at indicated pregnancy stages by administration of 5 mg/ml tamoxifen in corn oil X5 body weight by oral gavage. For harvesting of embryos, timed-pregnant females were euthanized by cervical dislocation. Plug date was defined as E0.5.

Staff and veterinary personnel monitored all mouse strains daily for health and activity. Mice were given ad libitum access to water and standard mouse chow with 12-h light/dark cycles. All animal procedures were approved by the Institutional Animal Care and Use Committee and performed in strict adherence to Weizmann Institute Animal Care and Use guidelines, following the NIH, European Commission, and Israeli guidelines. Tail genomic DNA was used for genotyping.

METHOD DETAILS

Cell isolation and flow cytometry

Single-cell experiments were performed on forelimbs from E10.5, E11.5, E12.5, E13.5 and E14.5 mouse embryos. For collection of E10.5 cells, *Sox9-GFP* and *Sox9-CreER^{T2}-tdTomato;ScxGFP* (without tamoxifen induction) mice were used. For collection of E11.5-E14.5 cells, *Sox9-CreER^{T2}-tdTomato;ScxGFP* mice were used 48 h after Cre induction.

Forelimbs were dissected and minced in cold PBS using small scissors. For each biological replicate, forelimbs of embryos from the same litter were pooled together (six forelimbs at E10.5 and E11.5, four forelimbs at E12.5 and E13.5, and two forelimbs from one E14.5 embryo). Forelimb tissues were dissociated using enzymatic digestion. E10.5-E11.5 forelimbs were digested with pre-heated 0.25% trypsin in DMEM medium (ThermoFisher) and incubated for 10 min at 37°C, gently pipetting every 3 min. E12.5-E14.5 forelimbs were digested with 1.5 mg/ml collagenase type V (Sigma-Aldrich) in DMEM at 37°C for 10-15 min, gently pipetting every 5 min until the tissue completely dissolved. The digestion reaction was stopped by addition of DMEM supplemented with 10% FBS and 1% Pen-Strep. Cell suspensions were filtered through a 40-μm nylon mesh and collected by centrifugation at 1000 rpm for 7 min at 4°C. Supernatant was removed and cells were resuspended in 500 μl ice-cold MACS buffer (with 0.5% BSA and 2 mM EDTA in PBS) and used immediately for FACS.

Flow cytometry analysis and sorting were performed using an AriaFusion instrument (BD Biosciences, San Jose, CA) equipped with 488, 407, 561 and 633 nm lasers, using a 100-μm nozzle. Sorting gates and fluorescence compensation were defined based on GFP, tdTomato single-stained and unstained control cells. Live cells were gated using DAPI staining (1 μg/ml) and by size and granularity using FSC-A versus SSC-A. FSC-W versus FSC-A was used to further distinguish single cells. Unstained, GFP-stained only and tdTomato-stained only cells were mixed in various combinations to verify that the analysis excluded false-positive doublets. GFP was detected by excitation at 488 nm and collection of emission using 502 longpass (LP) and 530/30 bandpass (BP) filters. tdTomato was detected by excitation at 561 nm and collection of emission using a 582/15 BPfilter. DAPI was detected by excitation at 407 nm and collection of emission using a 450/40 BP filter. Data were collected and analyzed using BD FACSDiva software v8.0.1 (BD Biosciences).

For single-cell RNA-seq,[101] live cells were sorted into 384-well cell capture plates containing 2 μL of lysis solution and barcoded poly(T) reverse-transcription primers. In each plate, four empty wells were used as a control. Immediately after sorting, each plate was spun down to ensure cell immersion into the lysis solution, snap frozen on dry ice and stored at −80°C until processed.

Massively parallel single-cell RNA sequencing (MARS-Seq)

FACS-sorted cells were used for single-cell library preparation according to MARS-seq protocol, as described in Jaitin et al.[101] Briefly, mRNA from cells sorted into capture plates was barcoded, converted into cDNA and pooled using an automated pipeline. The pooled sample was then linearly amplified by T7 *in vitro* transcription and the resulting RNA was fragmented and converted into sequencing-ready library by tagging the samples with pool barcodes and Illumina sequences during ligation, reverse transcription and PCR. Each pool of cells was tested for library quality and concentration was assessed as described in Jaitin et al.[101]

PACT clearing

For sample preparation, E9.5-E14.5 embryos were harvested from Bl6, *Msx1-CreER; Rosa26-tdTomato, Scx-GFP* and *Msx1-CreER^{T2}; Rosa26-tdTomato* timed-pregnant females and fixed in ice-cold 4% PFA in 1x PBS overnight. PFA-fixed embryos were dissected and forelimbs were cleared using PACT method.[103,104] Briefly, samples were washed in PBS, then incubated in hydrogel solution containing 4% (wt/vol) acrylamide in 1x PBS with 0.25% thermal initiator 2,2'-azobis[2-(2-imidazolin-2-yl)propane]dihydrochloride (Wako, cat. no. VA-044) at 4°C overnight. The next day, hydrogel was polymerized at 37°C for 3 hours. The samples were removed from the hydrogel, washed in PBS, and moved to 10% SDS with 0.01% sodium azide, shaking (60 rpm) at 37°C for 1-5 days, changing the SDS solution each day. Cleared samples were washed three times for 5 min with 1× PBST (PBS+ 0.1% Triton X-100 + 0.01% sodium azide) at room temperature and then subjected to whole-mount *in situ* HCR or whole-mount SOX9 immunostaining.

Please cite this article in press as: Markman et al., A single-cell census of mouse limb development identifies complex spatiotemporal dynamics of skeleton formation, Developmental Cell (2023), https://doi.org/10.1016/j.devcel.2023.02.013

Whole-mount immunostaining

To detect SOX9, samples were first incubated with proteinase K (Millipore Sigma, P9290) for 10 min at room temperature, washed and post-fixed again in 4% PFA. Then, samples were incubated with 5% goat serum, 1% BSA dissolved in PBST at 4°C overnight in order to block non-specific binding of immunoglobulin. Next, samples were incubated with primary anti-SOX9 antibodies (1:100, AB5535 Millipore Sigma) in 5% goat serum, 1% BSA dissolved in PBST shaking at 37°C for 5 days. Samples were washed four times for 2 h with 1× PBST at room temperature. Next, samples were incubated with secondary Cy5 antibodies (1:100, 715-165-150, Jackson ImmunoResearch) and 1:100 DAPI (1 mg/ml) in 5% goat serum, 1% BSA dissolved in PBST shaking at 37°C for 2 days. Samples were washed four times for 2 h with 1× PBST at room temperature and then prepared for light sheet imaging. To bring the refractive index (RI) of the sample to 1.45, it was submersed in a refractive index matching solution (RIMS) prepared by dissolving 35 g of Histodenz (Millipore Sigma, D2158) in 30 ml 0.02 M phosphate buffer, shaking gently at room temperature for 1-2 days. Finally, samples were embedded in 1% low gelling agarose (Millipore Sigma, A9414) in PBSin a glass capillary, submerged in RIMS and stored protected from light at room temperature until imaging.

Whole-mount *in situ* hybridization chain reaction (HCR)

The *Msx1* (NM_010835.2), *Shox2* (NM_001302358.1), *Hoxd13* (NM_008275.4) and *Sox9* (NM_011448.4) probes and DNA HCR amplifiers, hybridization, wash and amplification buffers were purchased from Molecular Instruments. *In situ* HCR v3.0 was performed using the protocols detailed in www.molecularinstruments.com. Briefly, PACT-cleared samples were pre-incubated with hybridization buffer and incubated overnight at 37ºC, 60 rpm with probe solution containing 1 μL of each probe in 250 μL of pre-heated probe hybridization buffer. The next day, probes were washed four times for 15 min at 60 rpm with pre-heated wash buffer, followed by two 5-min washes at room temperature with 5xSSCT. Next, samples were pre-amplified with 250 μL of amplification buffer for 5 min at room temperature and incubated with 250 μL of hairpin mixture (5 μL of hairpin h1 and hairpin h2 from 3 μM stock for each probe) overnight in the dark at room temperature. The following day, samples were washed with 5xSSCT two times for 5 min, two times for 30 min and once for 5 min at room temperature, gently shaking. For nuclear staining, samples were incubated with 1:100 DAPI/PBS solution (DAPI stock, 1 mg/ml) overnight at 4ºC, gently shaking. Finally, samples were washed twice with 2XSSC for 5 min at room temperature gently shaking and prepared for light sheet imaging as described above for SOX9-immunostained samples.

Light-sheet fluorescence microscopy

Samples were imaged with a Zeiss Lightsheet Z.1 microscope. For each limb, a low-resolution image of the entire limb was taken with the 20× Clarity lens at a zoom of 0.36. Light-sheet fusion of images was done if necessary in Zen software (Zeiss). Tile stitching and 3D image reconstruction were performed using Imaris software (Bitplane). For examination of *Msx1* lineage expression in skeletal elements, *Sox9* expression was used to generate the surface of the elements. Voxels outside the surface were masked using the mask function in Imaris software.

QUANTIFICATION AND STATISTICAL ANALYSIS

Low-level processing and filtering

RNA-seq libraries were sequenced by Illumina NextSeq500 at a median sequencing depth of 58,585 reads per single cell. Sequences were mapped to mouse reference genome (mm10), demultiplexed, and filtered as previously described by Jaitin et al.,[101] with the following adaptations. Mapping of reads was done using HISAT version 0.1.6[105] and reads with multiple mapping positions were excluded. Reads were associated with genes ifthey were mapped to an exon defined by a reference set obtained from the UCSC genome browser extended by up to 2 kb for complete 3' peak acquire. Noise level was estimated statistically on empty MARS-seq wells; median estimated noise over all experiments was 2%. Cells with less than 600 UMIs were discarded from the analysis. After filtering, cells contained a median of 2,800 unique molecules per cell. All downstream analysis was performed in R.

Metacells modeling

We used the metacells pipeline[33] with the following specific parameters (complete script reproducing all analyses from raw data is available in GEO: GSE185940). We removed mitochondrial genes, genes linked with poorly supported transcriptional models (annotated with the prefix "RP-") and cell cycle genes, which were identified by correlation coefficient of at least 0.1 for one of the anchor genes *Mki67*, *Hist1h1d*, *Pcna*, *Smc4*, or *Mcm3*. We then filtered cells with total fraction of mitochondrial gene expression exceeding 30% and cells with high (> 64) expression of hemoglobin genes (*Hba-a2*, *Hba-a1*, *Hbb-b2*, *Hba-x*, *Hbb-b1*). Feature genes for MetaCell analysis were selected if their scaled variance (variance divided by mean) was 0.2 and higher (T_vm=0.2), there were at least 100 UMIs across the entire dataset, and at least three cells with more than 4 UMIs recorded.

The gene selection strategy produced 425 marker gene features for the computation of the metacells balanced similarity graph. We used K = 150, 500 bootstrap iterations and otherwise standard parameters (500 iterations; resampling 70% of the cells in each iteration, and clustering the co-cluster matrix with minimal cluster size set to 20). We applied outlier filtering.

The resulting metacells model was annotated using the metacells confusion matrix and analysis of known marker genes. Muscle, epidermal, Schwann and immune metacells were excluded from further analysis. Next, we applied again the metacells pipeline on the remaining cells with the above-mentioned parameters.

Please cite this article in press as: Markman et al., A single-cell census of mouse limb development identifies complex spatiotemporal dynamics of skeleton formation, Developmental Cell (2023), https://doi.org/10.1016/j.devcel.2023.02.013

To annotate the resulting metacells into cell types, we used the metric $FP_{gene,mc}$, which signifies for each gene and metacell the fold change between the geometric mean of this gene within the metacells and the median geometric mean across all metacells, thus highlighting for each metacell genes that are highly overexpressed as compared to the background. Finally, we hierarchically clustered the FP most significantly changing gene table along with a set of known marker genes to identify the major cell populations.

Defining progenitor gene module signatures and scores

To define the gene signatures of progenitor cells, we first identified modules of co-expressed genes by Pearson's correlation across the metacells $\log_2 FP_{gene,mc}$ expression of the 175 most variable genes. The signature genes for each progenitor state were defined by module scores. Scores for each module were calculated per Metacell, by summing the log-normalized values over the genes in the module. Each gene contributed equally to the score in a sum of logs fashion.

Calculation of a chondrogenic score

To define a chondrogenic gene signature, we generated a list of genes correlated with *Col2a1*. To avoid over-fitting of the modeling, TFs were excluded from the list, which contained 84 genes. Chondrogenic scores were calculated per cell, by summing the log-normalized values over the genes in the set. Each gene contributed equally to the score in a sum of logs fashion. Cells were then stratified into 65 groups based on expression quantiles. To validate our approach, we tested differential expression of TFs that were not part of the signature gene set and are upregulated during chondrogenesis.

Slingshot analysis

To identify lineage trajectories and align metacells along pseudo-time we used a published package Slingshot.[106] For proximal cells, Slingshot was applied to P1 (naïve progenitors), P2 (proximal progenitors), C1 (proximal chondrocytes), C4 (attachment cells) and C6 (mature chondrocytes). For autopodial cells, Slingshot was applied to P1 (naïve progenitors) P3 (autopodial progenitors), C2 (autopodial chondrocytes), C3 (intermediate autopodial chondrocytes) and C5 (mature autopodial chondrocytes). The trajectory was inferred based on differentially expressed genes, defined as genes with more than 100 UMI, at least four cells with more than 4 UMIs recorded, and with variance of gene/ mean of gene > 0.2. Start or end points were not predefined.

Statistical analyses

Differential gene expression analysis was performed on $\log_2$ sum of UMIs normalized by reads per cell, divided by cell number. P-values were calculated using Wilcoxon test to compare between mean expressions of metacells (for Figures 2 and S2–S4) or cells (for Figure S3).